FRONTIERS OF CIVIL ENGINEERING AND DISASTER PREVENTION AND CONTROL

VOLUME 1

Edited by

Yang Yang and Ali Rahman

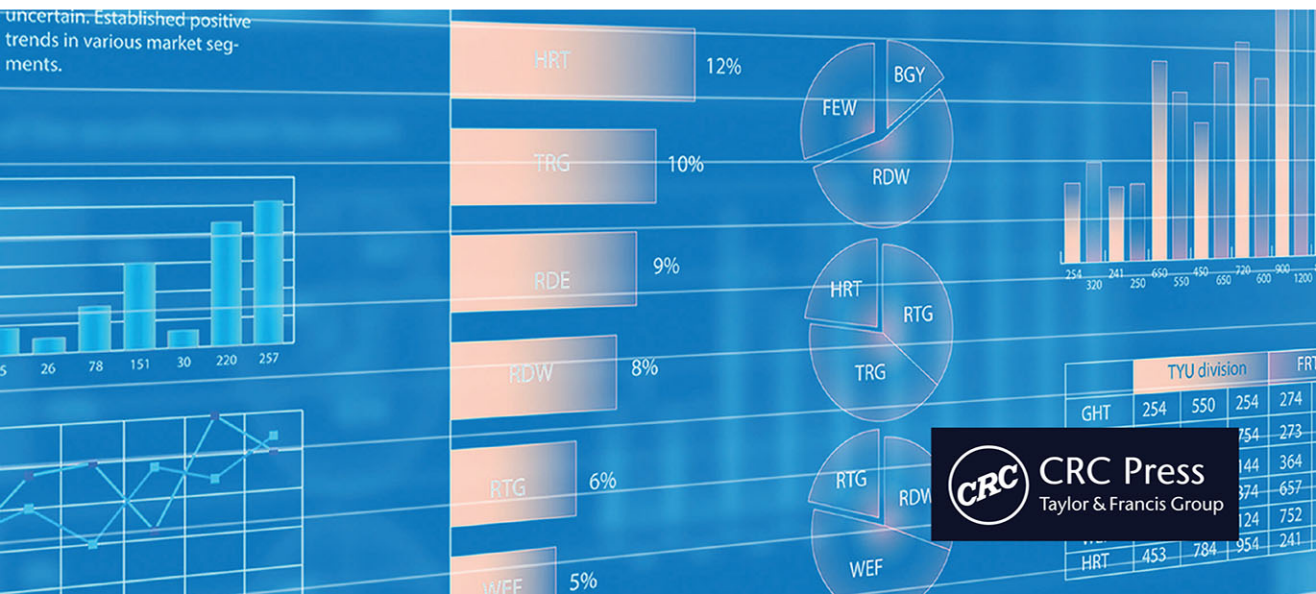

FRONTIERS OF CIVIL ENGINEERING AND DISASTER PREVENTION AND CONTROL VOLUME 1

Frontiers of Civil Engineering and Disaster Prevention and Control is a compilation of selected papers from The 3rd International Conference on Civil, Architecture and Disaster Prevention and Control (CADPC 2022) and focuses on the research of architecture and disaster prevention in civil engineering. The proceedings features the most cutting-edge research directions and achievements related to construction technology and prevention and control of disaster. Subjects in this proceedings include:

Construction Technology
Seismicity in Civil Engineering
High-Rise Building Construction
Disaster Preparedness and Risk Reduction
Smart Post-Disaster Rescue

These proceedings will promote development of civil engineering and risk reduction, resource sharing, flexibility and high efficiency. Moreover, promote scientific information interchange between scholars from the top universities, research centers and high-tech enterprises working all around the world.

Taylor & Francis
Taylor & Francis Group
http://taylorandfrancis.com

PROCEEDINGS OF THE 3RD INTERNATIONAL CONFERENCE ON CIVIL, ARCHITECTURE AND DISASTER PREVENTION AND CONTROL (CADPC 2022), WUHAN, CHINA, 25–27 MARCH 2022

Frontiers of Civil Engineering and Disaster Prevention and Control

Volume 1

Edited by

Yang Yang
Chongqing University, China

Ali Rahman
Southwest Jiaotong University, China

CRC Press
Taylor & Francis Group
Boca Raton London New York Leiden

CRC Press is an imprint of the
Taylor & Francis Group, an **informa** business

A BALKEMA BOOK

First published 2023
by CRC Press/Balkema
4 Park Square, Milton Park, Abingdon, Oxon OX14 4RN, UK
e-mail: enquiries@taylorandfrancis.com
www.routledge.com – www.taylorandfrancis.com

CRC Press/Balkema is an imprint of the Taylor & Francis Group, an informa business

ISBN: 978-1-032-39108-3 (SET hbk)
ISBN: 978-1-032-39111-3 (SET pbk)

ISBN Volume 1: 978-1-032-31200-2 (hbk)
ISBN Volume 1: 978-1-032-31201-9 (pbk)
ISBN Volume 1: 978-1-003-30857-7 (ebk)

DOI: 10.1201/9781003308577

ISBN Volume 2: 978-1-032-39103-8 (hbk)
ISBN Volume 2: 978-1-032-39106-9 (pbk)
ISBN Volume 2: 978-1-003-34843-6 (ebk)

DOI: 10.1201/9781003348436

Typeset in Times New Roman
by MPS Limited, Chennai, India

Frontiers of Civil Engineering and Disaster Prevention and Control – Yang & Rahman (Eds)
© 2023 The Editor(s), ISBN: 978-1-032-31200-2

Table of contents

Building material properties and highway bridge construction

Frontiers of Civil Engineering and Disaster Prevention and Control – Yang & Rahman (Eds)

Preface

Due to recent pandemic, the 3rd International Conference on Civil, Architecture and Disaster Prevention and Control (CADPC 2022) which was planned to be held in Guangzhou, China, was held virtually online during March 25–27, 2022. The decision to hold the virtual conference was made in compliance with many restrictions and regulations that were imposed by countries around the globe. Such restrictions were made to minimize the risk of people contracting or spreading the COVID-19 through physical contact. There were 120 individuals who attended this online conference, represented many countries including Malaysia, Iran, India and China.

CADPC 2022 focused on construction technology, disaster prediction, disaster prevention and control, and post-disaster reconstruction. The conference provided a platform for scholars from universities at home and abroad, researchers and engineers to share research results and cutting-edge technologies. All attendants get the chance to know about updated academic trends, develop new way of thinking, improve academic research and discussions, and promote industrialization of research findings.

During the conference, the conference model was divided into three sessions, including oral presentations, keynote speeches, and online Q&A discussion. In the first part, some scholars, whose submissions were selected as the excellent papers, were given about 5-10 minutes to perform their oral presentations one by one. Then in the second part, keynote speakers were each allocated 30-45 minutes to hold their speeches. In the second part, we invited four professors as our keynote speakers. Dr. Mohammadreza Vafaei, School of Civil Engineering, Faculty of Engineering, Universiti Teknologi Malaysia. His field of specialty and interest: Seismic design and rehabilitation, Structural health monitoring, Signal processing, Neural networks and Wavelet Transforms. And then we had Distinguished Professor. Zhifeng Xu. He delivered a wonderful speech: *Analytical approximations for the frequency response, localization factor and attenuation coefficient of one-dimensional periodic foundations.* Professor. Xinlin Wan, College of Civil Engineering, Anhui Jianzhu University. His research area: Geotechnical Engineering, Geophysical Exploration, Engineering Seismic, etc. Lastly, we were glad to invite Associate Professor. Deng Peng, College of Civil Engineering, Hunan University. He performed a speech on *Experimental Investigation of Seismic Uncertainty Propagation through Shake Table Tests.* Their insightful speeches had triggered heated discussion in the third session of the conference. Every participant praised this conference for disseminating useful and insightful knowledge.

The proceedings are a compilation of the accepted papers and represent an interesting outcome of the conference. Topics include but are not limited to the following areas: Civil, Construction Technologies, Disaster Prevention and Control and more related topics. All the papers have been through rigorous review and process to meet the requirements of international publication standard.

We would like to acknowledge all of those who supported CADPC 2022. The help and contribution of each individual and institution was instrumental in the success of the conference. In particular, we would like to thank the organizing committee for its valuable inputs in shaping the conference program and reviewing the submitted papers.

We sincerely hope that the CADPC 2022 turned out to be a forum for excellent discussions that enabled new ideas to come about, promoting collaborative research. We are sure that the proceedings will serve as an important research source of references and knowledge, which will lead to not only scientific and engineering findings but also new products and technologies.

The Committee of CADPC 2022

Taylor & Francis
Taylor & Francis Group
http://taylorandfrancis.com

Frontiers of Civil Engineering and Disaster Prevention and Control – Yang & Rahman (Eds)
© 2023 The Editor(s), ISBN: 978-1-032-31200-2

Committee members

Conference General Chair
Prof. Fuyou Xu, *Dalian University of Technology, China*

Local Organizing Chair
Dr. Yiding Zhao, *Yancheng Institute of Technology, China*

Technical Program Committee
Prof. Tetsuya Hiraishi, *Kyoto University, Japan*
Prof. Fauziah Ahmad, *Universiti Sains Malaysia, Malaysia*
A. Prof. Mohammadreza Vafaei, *Universiti Teknologi Malaysia, UTM, Malaysia*
Dr. Sadegh Rezaei, *Shargh-e Golestan Institute of Higher Education, Iran*
Dr. Haytham F.A. Isleem, *Tsinghua University, China*

Taylor & Francis
Taylor & Francis Group
http://taylorandfrancis.com

Civil construction technology and structural seismic reinforcement

Taylor & Francis
Taylor & Francis Group
http://taylorandfrancis.com

Frontiers of Civil Engineering and Disaster Prevention and Control – Yang & Rahman (Eds)
© 2023 The Author(s), ISBN: 978-1-032-31200-2

A layered finite element method for transient heat conduction of functionally graded concrete beams

Qiang Liu
School of Civil Engineering and Architecture, Nanchang Hangkong University, Nanchang, Jiangxi, P.R. China
Poly Changda Engineering Co. LTD, Guangzhou, Guangdong, P.R. China

Huihua Zhang*, Shangyu Han & Xiaolei Ji*
School of Civil Engineering and Architecture, Nanchang Hangkong University, Nanchang, Jiangxi, P.R. China

ABSTRACT: Functionally graded concrete (FGC) is a type of new concrete composite whose functions and properties change with the spatial position. In this paper, a finite element model of the FGC beam is established with the idea of the layered model and the finite element software Ansys. A benchmark example is used to verify the feasibility and accuracy of the model for transient heat conduction, and the results show that the present solutions are in good agreement with the reference ones. Furthermore, the transient heat conduction of an FGC beam is analyzed and the influence of the gradient parameter on the temperature field is obtained.

1 INTRODUCTION

It is well known that traditional concrete has several defects, such as heavy self-weight, poor crack resistance, and complex field construction. In addition, the design idea of FGC is derived from functionally graded materials (i.e., FGMs, whose components and properties change continuously in space (Koizumi 1997). Compared with traditional concrete, FGC is superior in many aspects, e.g., mechanical properties, impermeability, fire resistance, and corrosion resistance (Evangelista et al. 2009; Gao et al. 2007). Due to excellent performance, it has been used in some practical projects. Considering the fact that there is not only mechanical load but also temperature load (temperature gradient generated by hydration heat, drastic change of ambient temperature, etc.), it is of great scientific and practical significance to study the thermal behavior of FGC, especially in the transient state.

The current studies on FGC mainly focus on the mechanical properties (Mastali et al. 2015, Moghadam & Omidinasab 2020), while the thermal behavior is rarely involved. Some representative work about thermal analysis are as follows: Wang et al. (2017) experimentally obtained the variation law of temperature, stress, and strain of FGC beam with the layer thickness of ultra-high performance concrete, based on concrete hydration heat. Zhang et al. (2018) used the finite element method (FEM) to analyze the thermal buckling and post-buckling of FGC plates.

To the authors' knowledge, there is no report on the transient heat conduction of FGC beams. Further, with regard to the advantages of FEM (i.e., high applicability, low cost, and easy parametric analysis), this paper combines FEM with the layered model (Huang et al. 2005) to explore the influence of material gradient parameters on the transient heat conduction behavior of FGC beams.

*Corresponding Author: hhzhang@nchu.edu.cn

DOI 10.1201/9781003308577-1

2 TRANSIENT HEAT CONDUCTION EQUATIONS OF FGC

Consider the physical domain Ω composed of 2D isotropic FGC shown in Figure 1. Ω is enclosed by the contour $\Gamma = \Gamma_1 \cup \Gamma_2$, with Γ_1 and Γ_2, respectively, the temperature boundary and the heat flux boundary. The differential governing equation of this problem is (Wang 2003):

$$\frac{\partial}{\partial x_1}\left(k(\mathbf{x})\frac{\partial T(\mathbf{x},t)}{\partial x_1}\right)+\frac{\partial}{\partial x_2}\left(k(\mathbf{x})\frac{\partial T(\mathbf{x},t)}{\partial x_2}\right)+Q=\rho(\mathbf{x})c(\mathbf{x})\frac{\partial T(\mathbf{x},t)}{\partial t} \tag{1}$$

where ∂ denotes partial derivative; k, ρ, and c are the thermal conductivity, the density, and the specific heat, respectively, at a constant pressure of the FGC, and may vary spatially with $\mathbf{x}=(x_1,x_2)$; T, t, and Q are the temperature, the time, and the heat source, respectively.

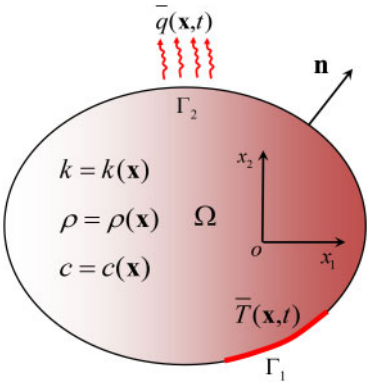

Figure 1. Transient heat conduction in a domain composed of isotropic FGC.

The corresponding boundary conditions are:

$$T(\mathbf{x},t)=\overline{T}(\mathbf{x},t) \quad \text{on} \quad \Gamma_1 \tag{2}$$

$$-k(\mathbf{x})\frac{\partial T(\mathbf{x},t)}{\partial x_1}n_1-k(\mathbf{x})\frac{\partial T(\mathbf{x},t)}{\partial x_2}n_2=\overline{q}(\mathbf{x},t) \quad \text{on} \quad \Gamma_2 \tag{3}$$

where $\overline{T}$ and $\overline{q}$ are the given temperature on Γ_1 and the heat flux on Γ_2, respectively; $(n_1,n_2)=\mathbf{n}$ is the outward unit normal to Ω. Moreover, the initial condition is $T(\mathbf{x},t)|_{t=0}=T_0(\mathbf{x})$.

3 FINITE ELEMENT EQUATIONS FOR FGC

By virtue of the Galerkin method and Equations (1)–(2), the following formula can be obtained (Wang 2003):

$$\int_\Omega \left[\begin{array}{l}\delta T(\mathbf{x},t)\left(\rho(\mathbf{x})c(\mathbf{x})\dfrac{\partial T(\mathbf{x},t)}{\partial t}\right)+\dfrac{\partial \delta T(\mathbf{x},t)}{\partial x_1}\left(k(\mathbf{x})\dfrac{\partial T(\mathbf{x},t)}{\partial x_1}\right)\\ \quad+\dfrac{\partial \delta T(\mathbf{x},t)}{\partial x_2}\left(k(\mathbf{x})\dfrac{\partial T(\mathbf{x},t)}{\partial x_2}\right)-\delta T(\mathbf{x},t)\rho(\mathbf{x})Q\end{array}\right]d\Omega-\int_{\Gamma_2}\delta T(\mathbf{x},t)qd\Gamma=0 \tag{4}$$

where δ is the variational symbol.

When modeled by the FEM, the physical domain Ω is first discretized into finite elements, and then the temperature in the element is approximately interpolated by the node temperature T_i of

this element, i.e.,

$$\widetilde{T} = \sum_{i=1}^{n_e} N_i(\mathbf{x}) T_i(t) \tag{5}$$

where N_i is the shape function at node i and n_e is the node amount attached to the element.

By substituting Equation (5) into Equation (4), and further considering the arbitrariness of the variation, the FEM global equations for 2D transient heat conduction problems in the FGC can be deduced as (Wang 2003):

$$\boldsymbol{C}\dot{\boldsymbol{T}} + \boldsymbol{K}\boldsymbol{T} = \boldsymbol{P} \tag{6}$$

where $\boldsymbol{C}$ is the heat capacity matrix, $\boldsymbol{K}$ is the heat conduction matrix, $\dot{\boldsymbol{T}} = dT(\mathbf{x}, t)/dt$ is the derivative array of node temperature with respect to time, and $\boldsymbol{P}$ is the array of temperature load. The details of $\boldsymbol{C}$, $\boldsymbol{K}$, and $\boldsymbol{P}$ can be found in Wang (2003).

4 LAYERED MODEL OF FGC BEAM

Because the finite element software Ansys finds it difficult to directly represent the continuous gradient change in FGC, the layered model (Huang et al. 2005) is used. Taking Figure 2 as an example, in the layered model, the FGC is divided into N parts, in which the material parameters of each layer are different, but those in the same layer are constant; i.e., FGC is regarded as a combination of N-layer-homogeneous materials.

Assume that the material properties of FGC are exponential along y-axis as shown in Figure 2, i.e.,

$$S(y) = S_0 e^{\beta_S y} \quad (S = k, \rho, c) \tag{7}$$

where S_0 is constant and β_S is the gradient parameter. From the idea of the layered model, and taking the center of each layer as the benchmarking, the material parameters of any homogeneous layer can be expressed by

$$S(i) = S_0 e^{\frac{\beta_S l(2i-1)}{2N}} (i = 1, 2, \ldots, N) \tag{8}$$

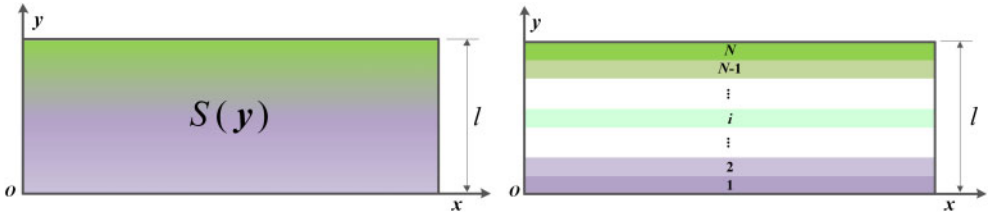

Figure 2. Theoretical (left) and layered model (right) of FGC.

Theoretically, the more the number of layers, the closer it is to the actual material. However, many layers will lead to lower calculation efficiency. Therefore, Section 5 discusses the determination of layer number through a typical example.

5 NUMERICAL EXAMPLE

In this section, a benchmark problem is first examined to verify the feasibility and accuracy of the method, and then a parametric study is carried out around the transient heat conduction in an FGC beam.

5.1 *Transient heat conduction in an FGMs plate*

As shown in Figure 3, transient heat conduction in a square FGM plate of edge size L is considered. The material parameters are $k(\mathbf{x}) = k_0(1+\gamma x_1)^2$, $c(\mathbf{x}) = c_0(1+\gamma x_1)^2$ and $\rho(\mathbf{x}) = \rho_0$. The temperature on the left side of the plate is $\overline{T}(\mathbf{x},t) = 0$, while that on the right side is $\overline{T}(\mathbf{x},t) = T_r H(t)$, where $H(t)$ represents the Heaviside step function). Moreover, the other edges are adiabatic and the initial temperature is 0.

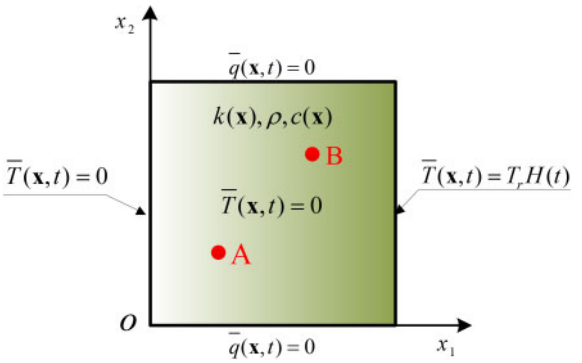

Figure 3. Transient heat conduction of square FGM plate.

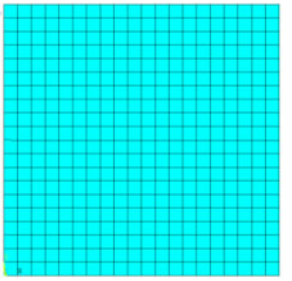

Figure 4. The finite element mesh corresponding to $h = 0.05$, $N = 20$.

According to the work by Sutradhar and Paulino (2004), the analytical solution of temperature field is represented as follows:

$$T(\mathbf{x},t) = \frac{T_1 x_1}{\sqrt{k}L} + \frac{2T_1}{\sqrt{k}} \sum_{n=1}^{\infty} \frac{\cos(n\pi)}{n\pi} \sin\left(\frac{n\pi x_1}{L}\right) \exp\left(-\frac{n^2\pi^2}{L^2}\kappa t\right) \tag{9}$$

where $T_1 = \sqrt{k_0}(1+\gamma L)T_r$ and $\kappa = k/(\rho c)$.

When modeling, we take $L = 1.0$, $k_0 = 5.0$, $c_0 = 1.0$, $\rho_0 = 1.0$, $\gamma = 2.0$, and $T_r = 100$. In the Ansys platform, the plate is discretized by Plane55 four-noded elements. The element size (edge length of a finite element) is, respectively, taken as $h = 0.2, 0.1, 0.05, 0.025$ and the corresponding number of divided layers is $N = 2, 10, 20, 40$. Figure 4 shows the finite element mesh when $h = 0.05, N = 20$ (the total number of elements is 400 and the total number of nodes is 441). In the analysis, the time step Δt is taken as 0.001. Tables 1 and 2, respectively, provide the simulated

Table 1. Temperatures of point A at different time, layer number, and element size.

N	$t\backslash h$	0.07	0.08	0.09	0.1
2	0.2	41.436	42.443	43.072	43.465
	0.1	41.469	42.475	43.099	43.486
	0.05	41.506	42.503	43.119	43.500
	0.025	41.515	42.509	43.124	43.504
10	0.1	52.777	54.056	54.850	55.342
	0.05	52.824	54.092	54.875	55.360
	0.025	52.836	54.100	54.882	55.364
20	0.05	52.895	54.466	54.951	55.437
	0.025	52.907	54.174	54.957	55.441
40	0.025	52.925	54.193	54.977	55.461
Exact solutions (Sutradhar & Paulino 2004)		53.198	54.387	55.112	55.555

Table 2. Temperatures of point B at different time, layer number, and element size.

N	$t \setminus h$	0.07	0.08	0.09	0.1
2	0.2	75.712	76.881	77.611	78.066
	0.1	75.709	76.892	77.626	78.081
	0.05	75.753	76.925	77.649	78.098
	0.025	75.764	76.933	77.655	78.102
10	0.1	78.877	79.973	80.652	81.073
	0.05	78.917	80.003	80.674	81.088
	0.025	78.927	80.010	80.679	81.092
20	0.05	78.957	80.044	80.715	81.131
	0.025	78.967	80.051	80.721	81.135
40	0.025	78.977	80.062	80.731	81.145
Exact solutions (Sutradhar & Paulino 2004)		79.209	80.225	80.846	81.224

temperatures of two sampling points, i.e., A: (0.3, 0.3) and B: (0.6, 0.6), as well as the analytical solutions by Equation (9). It can be found that with increase in the layer number and the refinement of the elements, the simulated results tend to be stable and closer to the exact solutions. However, the effect of the increasing layer number is more significant than that of element refinement on the improvement of solution accuracy. In addition, when the layer number is very small (e.g., $N = 2$), the simulated results are very unsatisfactory since the difference between the layered model and the actual one is very large.

5.2 *Transient heat conduction in an FGC beam*

Consider the transient heat conduction in an FGC beam as shown in Figure 5. The beam size is $L \times H$, and its material components are ordinary concrete and polypropylene fiber concrete (PPC). The bottom and top of the beam, respectively, correspond to pure PPC and pure ordinary concrete. The temperature at the bottom of the beam is $\overline{T_0}(x, y, t) = 0$, the temperature at the top is $\overline{T_1}(x, y, t) = T_R H(t)$, and the initial temperature is 20°C. The remaining boundary is insulated. It is assumed that the material parameters change exponentially along the y-axis, as shown in Equation (7).

In the simulation, we take $L \times H = 0.7$ m $\times$ 0.15 m, $T_R = 50$°C, thermal conductivity of PPC as $k_0 = 1.28$ W/(m · k) (Wang et al. 2014). and the thermal conductivity for ordinary concrete as $k_1 = 1.453$ W/(m · k) (Wang et al. 2014). Plane55 element is still used, the element size is 5 mm and the number of layers is $N = 30$. The corresponding finite element mesh is shown in Figure 6. The total number of elements and nodes are, respectively, 4,200 and 4,371. Because the density and specific heat of PPC and ordinary concrete are almost similar, the influences of density and specific heat between them can be ignored, and the unified value is $c = 913$ J/(kg · K) and $\rho = 2300$ kg/m^3. Further, we take time step $\Delta t = 50$ s.

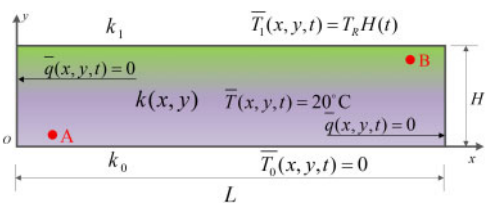

Figure 5. Physical model of FGC beam.

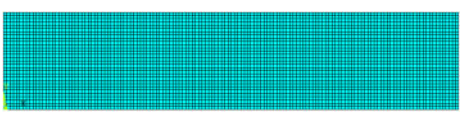

Figure 6. Finite element mesh in Ansys.

In this example, we mainly inspect the influence of the thermal conductivity gradient parameter on the temperature field of the FGC beam. Accordingly, the parameter $\beta_k H$ is taken as $\ln(1.453/1.28)$, $\ln(1.679/1.28)$, and $\ln(1.942/1.28)$, respectively. Figure 7(a) and (b) show the simulated temperatures of sampling points A: (0.1,0.02) and B: (0.6,0.12) at different times. It can be seen that the temperature of point A decreases, while that of point B increases with the increase in k. We can also view that during the initial period, the variation of temperature at different gradients of point A is undistinguishable, while that of point B is more obvious. Moreover, the temperature of both points gradually tends to be stable with the increase in time.

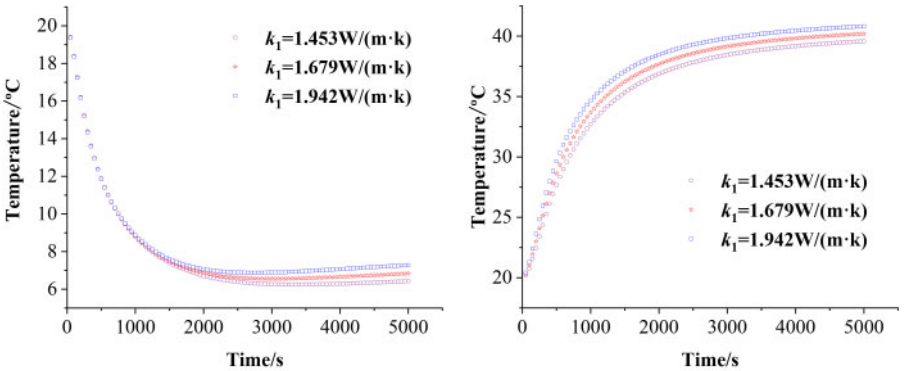

Figure 7. Simulated temperatures of sampling points at different time and material gradient.

6 CONCLUSIONS

In this paper, FEM in combination with the layered model is used to analyze the transient heat conduction of FGC. With the governing equation and boundary conditions of the problem, the corresponding finite element formula is derived by using the Galerkin method. A typical example is used to verify the feasibility, convergence, and accuracy of the proposed method. Based on this, the influence of material gradient parameters on the transient heat conduction of the FGC beam was further studied. The main conclusions were as follows:

(1) The proposed method can effectively address the transient heat conduction problem of FGC. In terms of solution accuracy, the more layers and elements are used, the higher calculation accuracy can be achieved. Moreover, the contribution of layer number is more significant than that of element refinement.
(2) The gradient change of thermal conductivity affects the temperature distribution, which indicates that the results given in this paper can provide some support for the component design of FGC under temperature loading.

ACKNOWLEDGMENTS

This work was supported by the National Natural Science Foundation of China (Grant No. 12062015 and 52068054) and the Provincial Natural Science Foundation of Jiangxi, China (Grant No.: 20212BAB211016).

REFERENCES

Evangelista, F., Roesler, J., Paulino, G.H. (2009) Numerical simulations of fracture resistance of functionally graded concrete materials. Transport. Res. Rec., 2113: 122–131.

Gao, Y.L., Ma, B.G., Wang, X.G., et al. (2007) Development and properties study on functionally graded concrete segment used in shield tunneling. Chinese Journal of Rock Mechanics and Engineering, 11: 2341–2347.

Huang, G.Y., Wang, Y.S., Yu, S.W. (2005) A new multi-layered model for in-plane fracture analysis of functionally graded materials (FGMs). Theoretical and Applied Mechanics, 01: 1–8.

Koizumi, M. (1997) FGM activities in Japan. Compos. Part B-Eng., 28(1–2): 1–4.

Mastali, M., Naghibdehi, M.G., Naghipour M., et al. (2015) Experimental assessment of functionally graded reinforced concrete (FGRC) slabs under drop weight and projectile impacts. Constr. Build. Mater., 95: 296–311.

Moghadam, A.S., Omidinasab, F. (2020) Assessment of hybrid FRSC cementitious composite with emphasis on flexural performance of functionally graded slabs. Constr. Build. Mater., 250: 118904.

Sutradhar, A., Paulino, G.H. (2004) The simple boundary element method for transient heat conduction in functionally graded materials. Comput. Method. Appl. M., 193(42): 4511–4539.

Wang, J.F., Zhang, Q., Du, H.X., et al. (2014) Thermal diffusivity research on polypropylene fiber reinforced high strength concrete (HSC) after high temperature. China Concrete and Cement Products, 12: 56–59.

Wang, K., Zhu, E., Li, B.D., et al. (2017) Effect of UHPC hydration heat on early age shrinkage cracking of functionally graded composite beams. Bulletin of the Chinese Ceramic Society, 36(01): 38–42.

Wang, X.C. (2003) Finite element method (second edition). Tsinghua University Press, Beijing.

Zhang, H.Q., Zhang, Z., Wu, H.L., et al. (2018) Thermal buckling and post-buckling analysis of functionally graded concrete slabs with initial imperfections. Int. J. Struct. Stab. Dy., 18(11): 1850142.

Frontiers of Civil Engineering and Disaster Prevention and Control – Yang & Rahman (Eds)
© 2023 The Author(s), ISBN: 978-1-032-31200-2

Research on the application of BIM technology in the design of prefabricated buildings and green construction

Xiaoqiang Tang*
Sichuan Aerospace Vocational College, Chengdu, Sichuan, China

ABSTRACT: With regard to "high energy consumption, high pollution, high waste, and low efficiency" caused by traditional construction methods used in different construction stages, this paper proposes "BIM technology as the support and core of prefabricated building." The "integrated" construction method realizes digital innovation in all aspects of construction engineering planning, design, construction, management, etc. Prefabricated building is an important innovation in the construction industry. It not only has the characteristics of specialization, standardization, and scale, but also meets the requirements of China's industrial structure adjustment and green energy-saving building evaluation standards, and has become the only way for the transformation and development of the construction industry. Prefabricated building technology can realize the integrated application and whole-process management of prefabricated buildings, improve operation and management efficiency, effectively reduce costs, save resources, and reduce risks; thereby, providing ensuring smooth implementation of prefabricated buildings. The digital upgrade of the construction industry has led to healthy and sustainable development of the industry.

1 INSTRUCTION

Currently, China has entered a new era of social development. The internal and external environment has undergone profound changes under this new historical reform. All industries and fields of the society are leveraging new opportunities and situations for development, but they will also be faced with new problems and new challenges. In an environment where economic development is shifting from a high-speed growth stage to a high-quality development stage, as an important industry in China's national economy, the construction industry actively seeks breakthroughs, conforms to the development trend of the industry, accelerates integration and innovation, and comprehensively realizes transformation and upgrading of high-quality development (Gao 2021). For a long time, China's construction industry has been affected by the application level of science and technology and the quality of employees, and most construction projects follow the traditional construction method of in situ pouring. Traditional construction methods have several shortcomings, such as high energy consumption, high pollution, high waste, low efficiency, and large errors in the process of practical application, and they are faced with the pressures of ecological environmental protection, labor costs, and rising building material costs, making it challenging to adapt to the construction. Developments in the new era of the industry call for new technologies and models to open up new directions for the traditional construction industry and rebuild new industry ecology. Prefabricated buildings are based on the prefabricated production of component factories and on-site prefabricated installation as an important form of modernization of the construction industry. They are characterized by standardized design, factory production, prefabricated construction, integrated decoration, and information management. Research and development, design, manufacturing, on-site assembly, and other business fields to achieve a new sustainable development of building products, energy-saving, environmental protection, and maximizing the full-cycle value of building production methods. (Wen 2020). Increase in prefabricated buildings not only has

*Corresponding Author: 304071943@qq.com

 DOI 10.1201/9781003308577-2

unparalleled advantages in engineering construction quality, construction work efficiency, cost consumption control, energy-saving, and environmental protection (as shown in Tables 1 and 2), but also brings a change in the overall craftsmanship and thinking mode of the industry. Since the "Twelfth Five-Year" Green Building and Green Ecological Regional Development Plan was issued by the Ministry of Housing and Urban-Rural Development in 2013, clear requirements of the current *"14th Five-Year" Development Plan for the Construction Industry* were mentioned for the first time, and prefabricated buildings entered the development stage rapidly. However, it can be seen that, as of 2021, the national prefabricated building penetration rate is at 14%, far lower than the mature markets in major countries in the world. As shown in Figure 1, the prefabricated building penetration rate in Japan and the U.S. is 90%. Fundamentally, weak technical support is an important reason behind the hindrance to the development of prefabricated buildings in China. Therefore, this paper believes that introduction of BIM technology into the design, production, construction, operation, and maintenance stages of prefabricated buildings can effectively improve the efficiency of collaborative designs of prefabricated buildings, reduce design errors, optimize the production process of prefabricated components, and improve the inventory management of prefabricated components. In addition, it may also help simulate and optimize the construction process, realize quality management and energy consumption management in the operation and maintenance stage of prefabricated buildings, and become the core for the application development of prefabricated buildings. It has made important contributions to the transformation and upgrading of the city and to healthy and green development (Yu 2021).

Table 1. Comparison of the advantages of prefabricated buildings and traditional buildings.

	Prefabricated building	Traditional building
Quality	The prefabricated construction method can better avoid quality problems such as water leakage, cracking, and large dimensional errors.	In the cast-in-place concrete structure, it is difficult to set up the formwork, the scaffolding is dense, and the forming quality is difficult to guarantee.
Energy-saving and environmental protection	Factory prefabrication can significantly minimize the high-altitude painting operation of workers' hanging baskets while also lowering safety risks. Prefabricated structures use less energy.	In traditional buildings, a lot of plastering, leveling, and wet work are required, which wastes materials and causes harsh construction environments.
Duration	Most of the components are completed in the engineering assembly line and are not affected by the weather. The overall delivery time is generally 30%–50% faster than the traditional one.	A more mature construction team can achieve one floor in five days for a structural project, but it also requires secondary structures such as bricklaying and plastering.

Table 2. Comparison of energy-saving and environmental protection data between prefabricated buildings and traditional buildings.

	Energy consumption per square meter (kg standard coal)	Water consumption per square meter (t)	Amount of garbage per square meter (t)
Prefabricated building	14.70	0.314	0.002
Traditional building	19.10	1.495	0.022

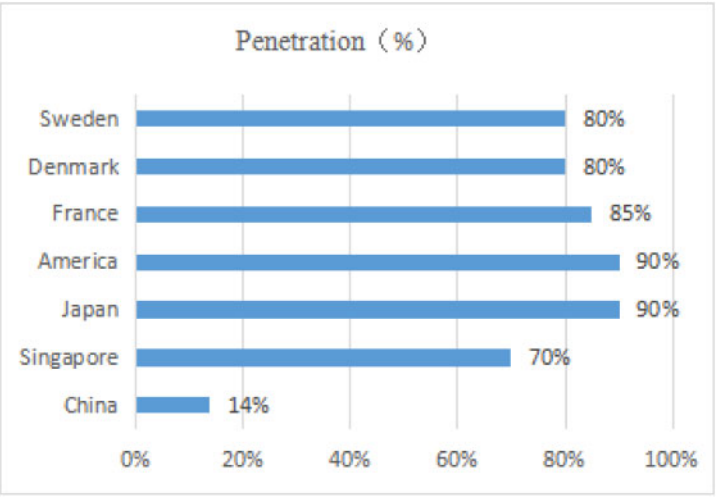

Figure 1. The penetration rate of prefabricated buildings in major countries in the world.

2 PREFABRICATED BUILDINGS AND BIM TECHNOLOGY

2.1 *Prefabricated building*

Prefabricated buildings refer to the transfer of a large number of on-site pouring operations in the traditional construction method to the factory, that is, to prefabricate various components or accessories for construction in advance, such as beams, columns, shear wall panels, stairs, etc. After being transported to the construction site, a suitable connection method is selected for different components or accessories to complete the assembly of the building. Prefabricated buildings can be classified according to different categories, including steel-framed buildings, wood-framed buildings, concrete-framed buildings, and composite buildings.

In terms of practical application, the concrete building type in the structural classification is the most common and widely used. Concrete structure buildings are mainly prefabricated concrete components (PC components for short), and the design, production, and construction of PC components are completed according to the shear wall structure system, frame structure system, or frame-shear wall structure system. Different structural systems have different characteristics, and their prefabricated components and scope of application also exhibit certain differences. Different building structures require different structural technical systems (He 2020). The selection of each structural technical system will include the determination of planning and design schemes, production standards for prefabricated components, on-site construction processes, and connection methods for PC components. It reflects the technical integration, refinement, and humanization of prefabricated buildings. Only by applying the appropriate technical system to the projects suitable for the use of prefabricated buildings can the advantages of prefabricated buildings be maximized and the purpose of improving construction quality, accelerating project progress, and improving the overall quality of construction projects. The benefits of prefabrication are fully reflected in the advantages of construction, energy savings, and environmental protection, preventing potential safety problems and enhancing the market link between supply and demand.

The prefabricated building integrates multiple links and processes, such as technical system research and development, overall design planning, factory manufacturing, prefabricated construction, operation and maintenance management, etc. It gradually improves and forms a set of overall technical solutions for prefabricated buildings in the development process. The prefabricated construction industry is in the process of transition from extensive to fine (Liao 2019). However,

we can see that the development of prefabricated buildings is still unsatisfactory under the current country's vigorous promotion and publicity of prefabricated buildings: Due to the rough design requirements in the general environment in the past 30 years in China. The Chinese people do not have higher requirements due to the mining-type construction method for refined and humanized building environment; key technologies need to be broken through, and the integration of design-production-construction-management is not enough. The adaptability is low and the molds and components between different projects are not common. The lack of modular design increases the project construction cost; lack of overall planning, single consideration of the design and development of each component or component, ignoring in-depth design, interior decoration design, and collaborative design. It is easy to have a huge impact on professional fields, such as structure, electromechanical decoration, and pipelines. Therefore, development of prefabricated buildings needs to achieve breakthroughs in key technologies on the basis of previous work, promote the application of networked and digital technologies in prefabricated buildings, master the key technical points of prefabricated components, and ensure that each process is completed. Smooth implementation to meet the specification requirements of the construction project.

2.2 *BIM technology*

Building Information Modeling is abbreviated as BIM, which is translated into Building Information Model in Chinese. The core of BIM is to use digital technology to complete the integration of data and information models of construction projects by establishing virtual three-dimensional models of construction projects and enabling models to be transmitted and shared with various links or processes in the entire life cycle of construction projects to facilitate the engineering and technical personnel and project managers to make accurate understanding and efficient processing of building information. At the same time, it also provides a platform for the exchange and sharing of engineering information among all participants in the construction project, thus laying the foundation for the realization of collaborative work in the construction project. As shown in Figure 2, the digital expression of the physical and functional characteristics of a construction project by BIM technology covers all stages of the construction project and runs through the entire life cycle of the construction project. As a result, BIM technology can be viewed as a comprehensive solution for realizing spatial digital informatization of construction projects, with data information serving as the core, an application model serving as the result, collaborative operation serving as the focal point, and a software program serving as the tool. BIM technology has entered a new stage (Zhang 2020).

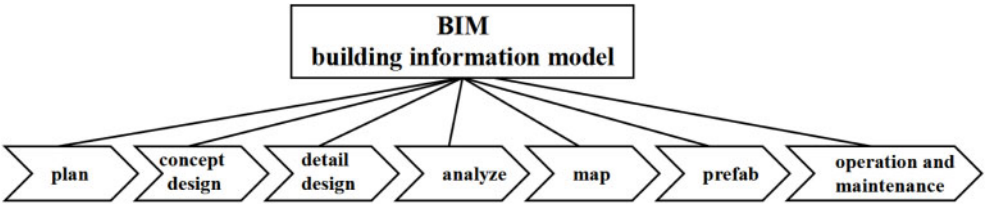

Figure 2. Features of BIM software.

The digital simulation of construction projects by BIM technology relies on three-dimensional digital technology. The content of a digital simulation is not only the building height, floor area, and external shape of the construction project, but also includes a large amount of auxiliary information, such as material strength, performance, security level, purchasing information, etc. In the actual operation process, 3D digital technology needs the support of software tools to build digital information models for successful engineering construction. The commonly used BIM modeling tools include the modeling software and related functional modules of Autodesk, Bentley, Nernetschek Graphisoft, and Gery Technology Dassault, as shown in Figure 3. Among them, Autodesk Revit

series software is commonly used, which is also the BIM model in China's construction industry. One of the most widely used software systems in the world is Autodesk Revit is an application that combines the capabilities of Autodesk Revit Architecture, Autodesk Revit MEP, and Autodesk Revit Structure software. After relying on the modeling software to establish the corresponding BIM model of the building structure, the BIM data model is analyzed and calculated in combination with the corresponding structural quality simulation analysis software. The commonly used simulation analysis software include PKPM, IES, Echotect, and Green Building Studio.

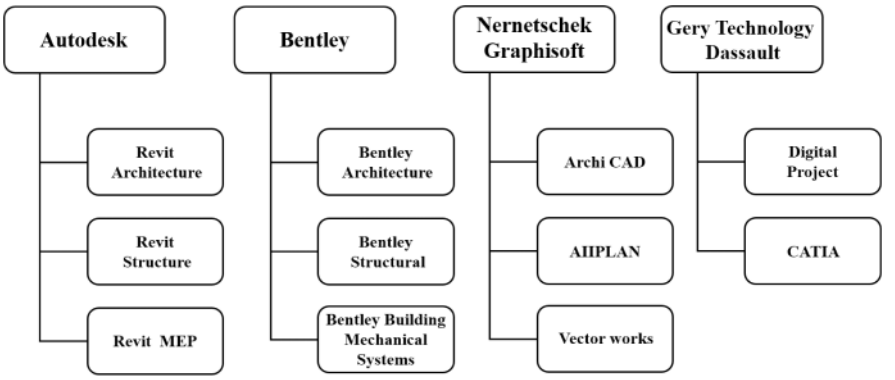

Figure 3. The most commonly used modeling software in BIM software.

Through BIM technology, a comprehensive database based on the three-dimensional digital information model can be constructed to realize the dynamic modification, adjustment, and storage of all data information for the construction project, thus realizing the coordination between the whole and each part of the engineering design process. Operation 3D digital information model under BIM technology can also help in the construction management stage of the project in the form of visualization. For example, through a large number of collision experiments, unreasonable places in the design can be quickly found and modified, to reduce the probability of safety accidents in actual construction and the probability of rework. Through the construction of the BIM digital information model, it is possible to make a statistical information table of the engineering quantity, the required quantity of each component, and the construction progress during the construction process, to further refine the control of the construction process of the construction project and realize the real environmental protection and energy-saving green construction, to avoid unnecessary waste of resources.

3 APPLICATION OF BIM TECHNOLOGY IN PREFABRICATED BUILDINGS

Prefabricated buildings have introduced new changes and developments in the construction industry, which not only significantly improve the construction efficiency but also promote the integration of the production of accessories into the construction industry (Qu 2019). However, prefabricated buildings also have problems and defects that need to be solved urgently. Prefabricated building technology dates much earlier than that of BIM technology, and the BIM technology, with its application characteristics of visibility, simulation, and coordination, has produced a strong degree of fit between the two, which can be combined with prefabricated building technology. The organic blending of construction technologies not only fulfills the complementing benefits of the two, but also breathes fresh life into prefabricated structures and even the whole construction sector, becoming an essential future growth trend.

3.1 *The application of BIM technology in the design stage*

In the planning and design stage of the prefabricated building, BIM technology is used to complete the architectural design. Compared with traditional CAD drawing, BIM software combines different data and complete simulation and quantification to form a three-dimensional digital model, which can provide designers with a detailed and scientific basis to complete the relevant design of construction projects. It can not only integrate multiple types of design drawings to improve design efficiency but also avoid subsequent repairs or repeated construction due to design errors during the project operation process and ensure design quality while controlling project costs. The BIM technology design process of prefabricated buildings is shown in Figure 4.

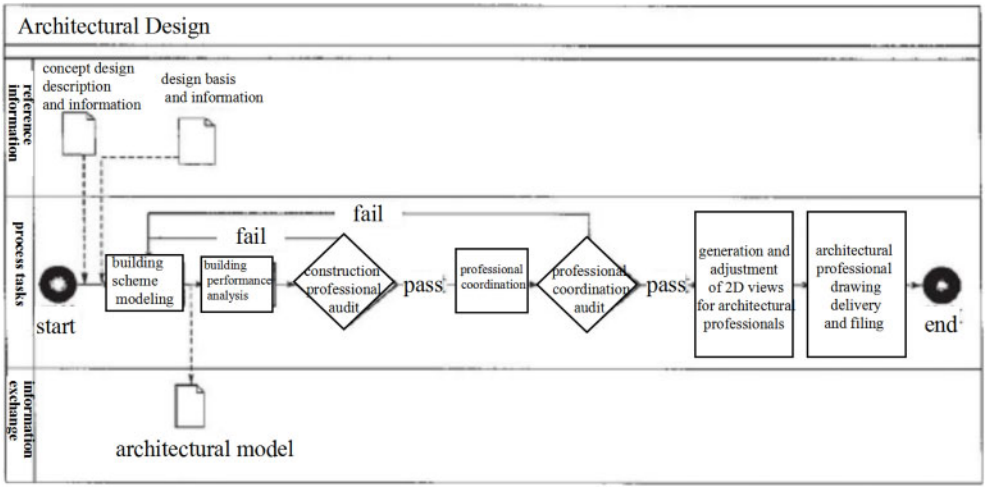

Figure 4. Architectural design phases based on BIM technology.

3.1.1 *Application of BIM technology in the early planning stage*

In the preliminary planning stage, after the data model of the overall building is constructed using BIM software, the corresponding analysis software is used to complete the relevant analysis of the construction project site in combination with the local environment, climate, and hydrological data. For example, in the planning and construction process of People's Hospital in a city along the southern coast, the solar and climate data of the place are collected with the help of relevant software, and based on the BIM model data, the relevant analysis software are used to conduct climate analysis, and the plan is then carried out, which include environmental impact assessment, comprising the impact of sunshine, wind, thermal environment, and acoustic environment (You 2019). Figure 5 shows the architectural model of the hospital building project, and Figure 6 shows the wind environment simulation of the main building of the hospital, which realizes the simulation and prediction of the normal distribution of indoor and outdoor airflow. The left side is for indoor ventilation, and the right side is for outdoor ventilation. According to various data, the building form and main structural system are optimized and adjusted in different aspects so that the architectural design scheme can achieve the best standard.

3.1.2 *Application of BIM technology in the detailed design stage*

After the prefabricated building design scheme is determined, it enters the deepening design stage. At this stage, BIM technology focuses on the processing of each node in the structural model—that is, to generate a component model that contains the data information attributes required for specific manufacturing. The detailed design of the component model is the key to the design of the prefabricated building. Professional designers collect design demand information, such as

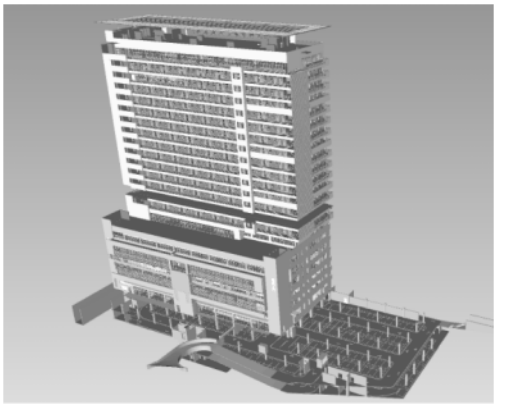

Figure 5. The main building model of the hospital.

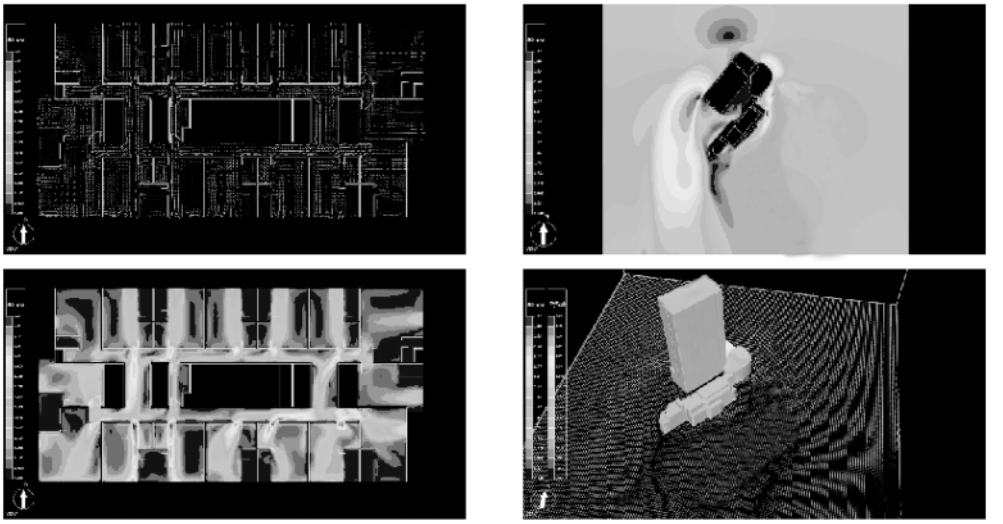

Figure 6. Site wind environment simulation test.

structure, water supply and drainage, HVAC, and power supply, and rely on the BIM technology platform to integrate the data and information to complete the solid design of the components. Compared with the plane drawing of CAD, BIM technology can complete the reinforcement work of components more intuitively, effectively reduce the error rate, and realize control of construction project cost. In addition, the three-dimensional model perspective under BIM technology supports the three-dimensional view of the construction, realizes the systematic design management of components, and improves the design completion and accuracy of prefabricated components.

3.1.3 *Application of BIM technology in collaborative design stage*

The design of prefabricated buildings is a comprehensive task that integrates multiple departments and disciplines. Various professionals in different departments need to carry out their work based on design drawings (models) and documents. This has resulted in a strong dependence between departments and personnel. On the one hand, various departments cooperate with each other to complete the design of the overall architectural plan; on the other hand, any modification in any

department affects all departments, making the problem more complex. The unified BIM platform built under the BIM technology ensures information exchange among various departments and majors. Using BIM technology and a BIM server, collaborative design is carried out on the same BIM model. Through collaborative design and visual analysis, it can be timely. Solving the inconsistency in the above design ensures smooth progress of the later construction (Yang 2016). In addition, in the collaborative design stage, the key aspect of the application of BIM technology is collision detection. That is, the contradictions and errors existing in the design of various departments and majors are automatically marked to facilitate the adjustment and modification of designers. After importing the BIM model into the collision-checking software, Navisworks, for analysis, it is discovered that there is a cross-connection between the water heating pipes and the air conditioning ducts in the hospital's main building, as shown in Figure 7, and the system will automatically identify and mark them to form the collision check result.

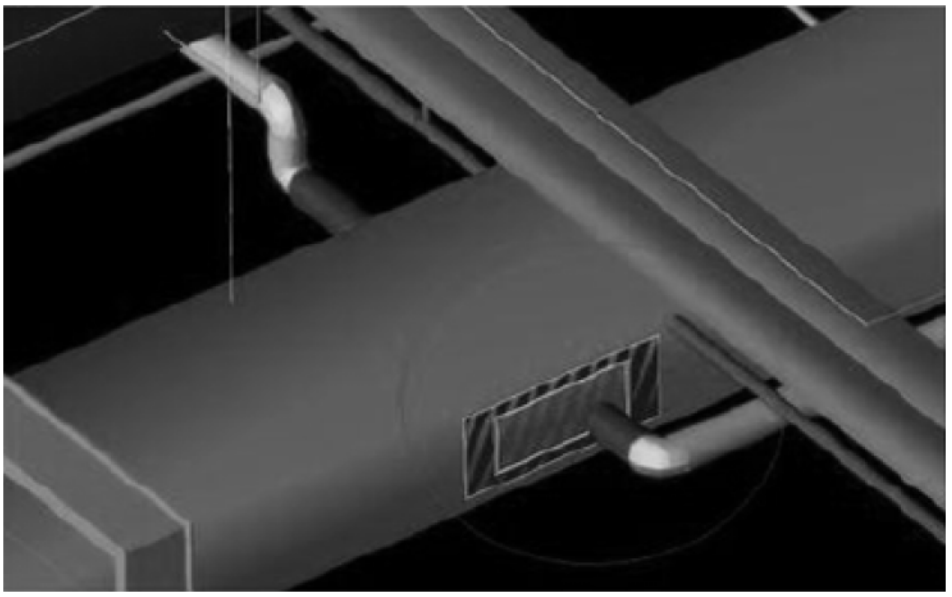

Figure 7. Display of the collision check result.

3.2 *Application in green construction*

Green construction is the general guiding concept that involves using prefabricated structures; however, in the actual construction process, issues such as insufficient construction management and substantial resource waste frequently have a direct impact on prefabricated building green construction evaluation outcomes. The aforesaid challenges may be successfully solved by applying BIM technology in prefabricated structures, and the needs of green construction can be really met.

3.2.1 *BIM technology to solve the problem of resource and energy waste*

First, in the construction stage of prefabricated buildings, construction managers can rely on BIM technology to generate a bill of quantities to achieve control over building resources and energy utilization. After the integration of the data and information models of the construction project, the attribute parameters of each component are automatically recorded by the BIM software system, and the corresponding family comprehensive database is automatically generated, and the shared parameters are established to generate the bill of quantities. Modifications and changes in the architectural design automatically change the bill of quantities. Second, it can clarify the details

and actual application of the materials required in each link of the construction and realizes the material consumption statistics according to the material list, to reduce the waste caused by not picking up materials as required. Finally, the application of BIM technology can also realize cost control in the construction process of prefabricated buildings. The established digital information model is combined with construction time, construction procedures, and other factors to form a multi-dimensional comprehensive information database, so that different departments and different professionals can update and collect the progress and cost in real time according to the actual project progress. Combined with the summary analysis function of BIM software, the cost analysis needs of the project can be met, and the summary and analysis of costs can be more convenient and rapid (Yuan 2021).

3.2.2 *BIM technology to solve the problem of comprehensive construction management*

The comprehensive management of the prefabricated building construction process ensures smooth completion of the construction project. Through the overall planning of construction projects, we can try our best to be environmentally friendly and finely control our progress to achieve the purpose of green construction of prefabricated buildings. The application of BIM technology can not only complete the design scheme of the prefabricated building, but also complete the simulation of the construction scheme and optimize the design of the construction scheme through continuous adjustments and modifications. Hence, BIM technology can add the construction schedule plan to the digital model to dynamically analyze the construction process and simulate the site conditions, as well as investigate potential problems in advance, arrange the construction site reasonably, do a good job of dispatching equipment and personnel, and ensure adequate construction safety measures (Tian 2017). For example, in the planning and construction process of the People's Hospital in a city along the southern coast above, after using BIM software to complete the architectural design, Aotodesk Naviswork was used to add the specific construction schedule to the digital model to form a 4D construction model, and using BIM to carry out construction simulation to enhance the construction management and control of the main building of the People's Hospital as a whole. As shown in Table 3, the grid plan for the construction progress of the main building of the People's Hospital can intuitively reflect the node relationship and the duration of each process in

Table 3. Plans for the construction of the main building of the people's hospital.

	Construction details (day)							
	1	2	3	4	5	6	7	8
I construction section wall hoisting	–							
II construction section wall hoisting		–						
I construction end sleeve simple grouting		–						
II Construction end sleeve grouting			–					
I construction section wall hoisting			–					
IV construction section wall hoisting				–				
Sleeve grouting in construction section II				–				
Sleeve grouting in construction section IV					–			
Post-casting with steel bar binding		–	–	–	–			
Post-casting with support formwork reinforcement		–	–	–	–			
Support frame erection		–	–	–	–			
Stacked beam hoisting					-			
Laminated board hoisting					–			
Pre-buried water and electricity pipelines					–	–		
Reinforcement of hanging formwork and anti-sill support Formwork at the drop plate							–	
Concrete pouring								–
Stair hoisting					–			

the construction process, further improving the control of the construction progress. In addition, it is also possible to find out possible problems in the construction through simulation and propose corresponding feasible adjustment plans to avoid potential safety hazards in time and increase the safety of project construction.

4 CONCLUSION

This paper proposes a comprehensive solution to the problems of "high energy consumption, high pollution, high waste and low efficiency" existing in the traditional construction mode of the current construction industry. Supported by BIM technology, the "integrated" construction method with prefabricated building technology as the core realizes digital innovation in all aspects of construction project planning, design, construction, management, etc., with the management covering the entire life cycle of construction projects as the foundation, focusing on improving the operation efficiency in the planning and design stage and improving the detail control in the construction stage, to achieve the standards of green design and green construction. The combination of BIM technology and prefabricated buildings not only realizes the standardization, systematization, and industrialization transformation and upgrading of the traditional construction industry, but also signals that the final development of the construction industry moves toward a green and low-carbon direction.

REFERENCES

Gao Fan. (2020). During the "14th Five-Year Plan" period, the transformation and upgrading of traditional buildings to smart buildings. Informatization of China Construction.

He Qiang. (2019). Research on new-type prefabricated building construction technology based on PC components. Construction & Design for Project.

Liao Liping.(2019). Development status and strategies of green prefabricated buildings. Enterprise Economy.

Qu Lipeng. (2019). Application exploration of BIM technology in prefabricated building design and construction management. China University of Mining and Technology.

Tian Dongfang. (2017). Research on the application of BIM technology in the construction management of prefabricated housing. Hubei University of Technology.

Wen Linfeng, Liu Meixia. (2020). Actively promote prefabricated buildings and promote high-quality development of the construction industry. Construction Science and Technology.

Yang Qilin. (2016). Research on the application of visual collaborative design based on BIM. Southwest Jiaotong University.

You Qian. (2019). On the role of BIM in various stages of the project. Jushe.

Yu Jing. (2021). Independent BIM technology promotes the transformation, upgrading and high-quality development of the construction industry. Informatization of China Construction.

Yuan Yuan. (2021). Application analysis of BIM in the design of prefabricated residential buildings for green energy saving. Building Technology Development.

Zhang Juxian. (2020). Research on the application of BIM technology in the whole life cycle of prefabricated buildings. Chongqing Architecture.

Frontiers of Civil Engineering and Disaster Prevention and Control – Yang & Rahman (Eds)
© 2023 The Author(s), ISBN: 978-1-032-31200-2

Research on ventilation ecological building design under regional influence

Zhang Yin* & Zhou Qi
School of Art and Design, Wuhan Institute of Technology, Wuhan, Hubei, China

ABSTRACT: Natural ventilation is one of the most commonly used methods in ecological building design. This paper cites several typical cases to illustrate the application of natural ventilation for green buildings in various regions, and finally proposes several measures for natural ventilation design. Its design process should be combined with geographical factors, humanistic history, economic conditions, etc.

1 INTRODUCTION

A building has a long service life because it is a consumable item built with a lot of of time and effort. Therefore, when planning a construction project, a rigorous design must be planned, considering the long-term problems that could arise in the future, with ecological concepts incorporated. Buildings used to be regarded as being energy intensive. The designs of diversified energy-saving devices have gradually gained people's attention (Wang 2020). During the 19th National Congress of the Communist Party of China, new requirements were laid out for constructing ecological civilizations, as well as the timetable and roadmap for building a beautiful China in the new era. To realize ecological civilization and build new-age China, it is necessary to establish the fundamental concept of harmonious coexistence between man and nature, adhere to strict environmental protection policies, and accelerate the reform of the ecological civilization system (Wang 2020). This indicates that the ecological problems in architecture industry are closely connected to the political, economic, and other issues that contribute to the development of a nation.

The ecological theme of buildings involves addressing the problem of building energy consumption. Buildings have diverse styles based on geographical conditions, but their core functions largely remain the same. Given this context, it is critical to explore the concepts and methods of building and natural ventilation design. It is envisaged that the findings of this study would inspire the construction of natural ventilation ecological buildings.

2 THE NEED FOR NATURAL VENTILATION

High-rise buildings thrive as cities grow, but some architects seek high-rise building designs with particular aesthetics, and natural ventilation has been a vital technological method for the betterment of people and the environment since long. Many ancient Chinese structures, such as ventilation, inner courtyards, and quadrangle courtyards, reflect its shadow (Li 2006). Natural ventilation, as a measure to minimize indoor heat, may accelerate the circulation of air within the building and disperse the temperature of the human body surface, thereby cooling the inside of the building at an era when electric power technology was not completely utilized.

*Corresponding Author: 809895605@qq.com

 DOI 10.1201/9781003308577-3

The basic principle of today's existing advanced ecological building strategies is to cut the building from the external space, and use advanced technology and equipment to solve the problem of building energy consumption. However, this so-called ecological strategy increases the engineering cost at the beginning of construction. The cost would be high, and if this building is not used for a long time in the future, this strategy will be "putting the cart before the horse".

Compared with other ecological technologies, natural ventilation is a low-cost and relatively mature technology system. Natural ventilation is a technology that exchanges interior and outdoor air by depending on natural air pressure or temperature differences rather than mechanical energy (Chen & Ye 2021). The purpose of achieving ecological protection with the least number of resources applies to the ecological environmental protection concept of the national policy and is in line with the national sustainable development strategy. Under the national conditions, under the "ecological environment" policy, the issue of architecture and ecology has been given much attention by architects, and the ecological architecture strategy utilizing natural ventilation is widely used by designers.

3 APPLICATION CASE OF VENTILATION BUILDING UNDER REGIONAL INFLUENCE

3.1 *Arizona state university*

3.1.1 *Background factor research*

Arizona State University (ASU) is located in the Phoenix metropolitan area. It is a top research university. The school is highly valued by the government as well as school leaders. Therefore, the teaching building will be used for a long time in the future. A point to consider is the significance of campus strength has prompted an increase in the number of students on campus, which in turn raises important questions about how the campus can develop sustainably in the future (Figure 1).

Figure 1. School location (created by the authors).

Geographical Background Facts: Arizona State University is located in the urban area of Phoenix, which belongs to the tropical desert area. It exhibits a typical subtropical continental arid and semi-arid climate. The rainy season is short, and the most common green plant is cactus. The tropical desert climate is characterized by sunshine, especially strong sunshine, a dry and hot summer, a large temperature difference between day and night, and more wind and sand. There are no abundant clouds in the sky, and the sun shines directly on the ground all year round, which makes part of the sun unstoppable and not very friendly. Because the weather is hot, dry, and with less rainfall, there is no water in the ground, and it is impossible to evaporate and cool down. Therefore, the

temperature in summer is particularly high, and the temperature difference between day and night is particularly significant, which poses a potential threat to the living (Figure 2).

Figure 2. Natural environment (source: network).

3.1.2 *Ventilation and eco-design applications*

Strategy 1: Ecological sustainability is a key design driver throughout the process. Tooker House at Arizona State University is a brand new seven-story 4.58 million sq. ft living and learning facility space for students. The architectural design layout of the teaching building is in the form of "one divided into two". The entire building complex is composed of two irregular rectangular volumes. The connecting bridges between the two buildings connect the circulation of people. So as to ensure the convenience of passage. And the connecting corridor bridge is made of perforated material. This special material can promote the passage of natural wind inside the building and form a "window through the hall". Compared with the traditional closed two-building form, this kind of ventilation corridor ensures that the building will not be damaged. It will block the natural wind flow, reduce the wind resistance of the building, and achieve the effect of allowing the smooth passage of tropical sand.

In addition, the composition of the building volume of the teaching building has been carefully calculated and planned by the designers. The entire building complex faces the east-west direction and is placed in a parallel position. The east-west high walls provide maximum shade for the site and its large openings. It has excellent lighting and powerful ventilation on the south and north sides, so it can also have sufficient sunshine in winter, which is helpful in maintaining the inside temperature (Figure 3).

Strategy 2: The design of the teaching building itself also promotes the movement of wind. People are accustomed to the traditional ventilation method of opening windows. In terms of simple ventilation, one of the buildings makes use of an algorithm to combine with the position of each window on the outer wall to form a unique curvilinear and wavy appearance. Opening and closing with changing weather conditions ensures proper control of sunlight entering the room, thus avoiding considerable energy consumption caused by strong sunlight. On the other hand, the perforated metal panels of this structure can drive the passage of natural wind and promote the improvement of indoor space. Air flow reduces indoor thermal effects, reduces the use of mechanical energy for ventilation and air conditioning, and saves building energy consumption. The materials used in the building walls are all local materials, which are like the roots of a tree deeply rooted in the soil. They are original and regional, giving people a visual sense of security and intimacy.

Affected by natural factors, strong winds will be blocked by the building, and the acceleration of the wind speed will lead to negative pressure in the building. The building adopts the overhead mode of the first floor to effectively relieve this pressure and allows the airflow to pass through the planned route, which is beneficial to the overhead layer. The evacuation of harmful gases from the parking lots from both sides, while providing the function of ventilation and noise reduction for the entire building complex in summer, can improve the impact of the desert climate (see Figure 4).

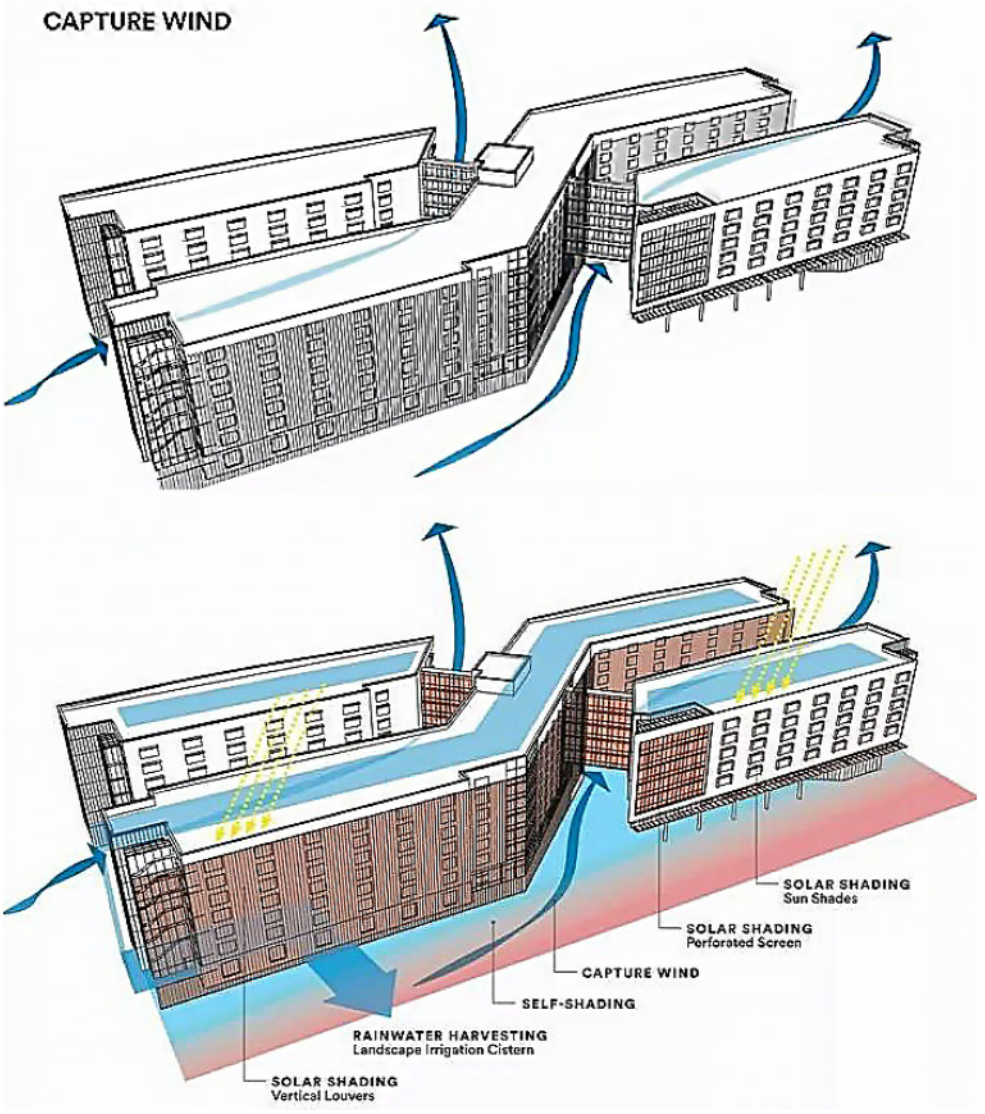

Figure 3. Buildings with two sky bridges (source: network).

3.2 *Star city shopping center, Wuhan, China*

3.2.1 *Background factor research*

Social background factors: Wuhan Qunxingcheng Shopping Center is located on Xudong Street, Wuchang District, Wuhan City, Hubei Province. Wuhan has nine provinces. Wuhan's superior geographical location created a prosperous atmosphere in Wuhan and promoted the development of commercial groups. People have an innate closeness to nature and yearn for a free blue sky and white clouds, mountains, rivers, streams, green trees, and flowers. The designer used this concept into the design of the building. At the same time, based on this group of star city shopping malls, they have rich visual impact (Figure 5).

Figure 4. A model for building facades (source: network).

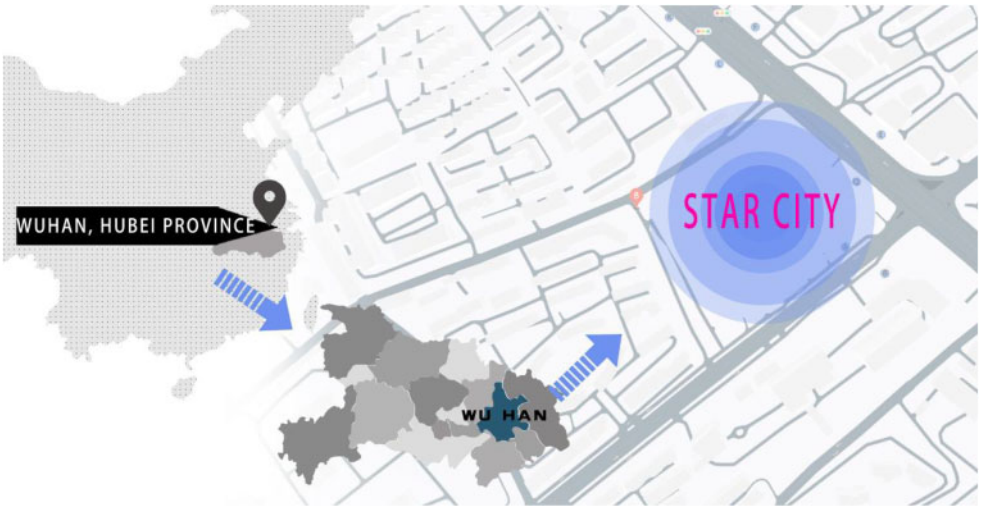

Figure 5. Analysis of geographic location (created by the authors).

Humid subtropical monsoon (humid) climate with abundant rainfall and sufficient heat in summer, rain and heat in the same season, and light and heat in the same season is typical of Wuhan.

The end of 2019 to the beginning of 2020 was a difficult period for people in facing the challenges of the pandemic. Although the spread of the disease has been effectively prevented and controlled, people are still urged to reduce crowd gatherings and confined spaces. Due to the relatively airtight environment in the building, coupled with various human activities, the air quality in the building is poor. Based on this, major business circles have implemented measures to switch off the central air conditioner to prevent the spread of virus that can aggravate by the circulating air. This goes back to the building itself, whether it can shoulder its mission and play a huge role in the epidemic.

3.2.2 *Ventilation and eco-design applications*

During the initial design stages of the architecture, the idea of nature was taken as the central motif, with the "canyon" as its design form. A "garden-style" shopping center has been created by integrating natural elements with the architectural environment. At the same time, it is important to consider ecological effects.

In the design of the façade, Wuhan's Qunxingcheng Square combines the concept of mountains and canyons to show the rock formation curves of the canyon through wooden textures (Figure 6). The open atrium is designed with reference to the topography of the canyon, creating an external

feature of mountains, introducing the stream trail in the canyon to create a vertical "waterfall" landscape of the building, and the layers of plants on the platform are the air. A three-dimensional vertical atrium space designed to supplement oxygen and reduce atmospheric particles is surrounded by green plants and flowing water, creating a pure natural atrium exhaust system.

Figure 6. External of Qunxingcheng Square (Source: network).

In the ventilation system of the atrium, the natural wind can penetrate into the indoor space of each floor of the building, so that the air is circulated inside the originally airtight building, which is a natural method to realize the conversion of indoor and outdoor air. After the epidemic, natural ventilation is an important protective measure to effectively alleviate the retention and accumulation of indoor bacteria and harmful gases. It may be possible to reduce the virus concentration in the air by implementing protective ventilation measures, thereby minimizing the overall exposure of users to viruses (Figure 7).

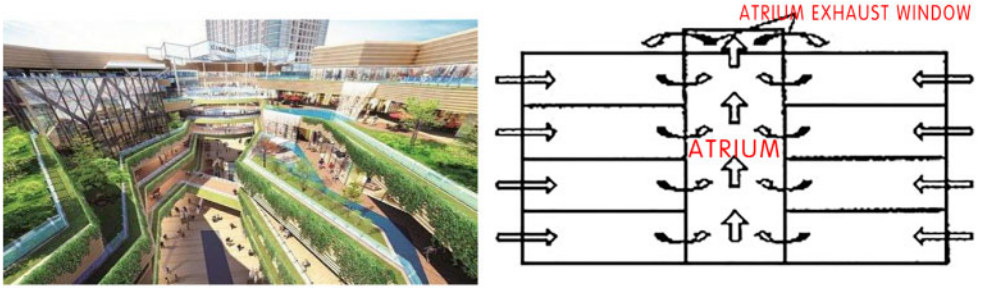

Figure 7. Atrium space of Qunxingcheng Square (source: network).

3.3 *Chengdu dayi agricultural science base exhibition center*

3.3.1 *Background factor research*

Chengdu Pastoral Resort is home to the Dayi Agricultural Science Base Exhibition Center. Under the background of national rural revitalization, breaking the dual structure of urban and rural areas, and tracing the roots of the city to the countryside, we create a western Sichuan Linpan with pastoral hotels (homestays) as the core and popular science, children, theme parks, and health care cultural experiences as the content of activities (Xie & Ruan 2020). This pastoral complex, to inherit and carry forward the traditional culture of western Sichuan, continues the architectural style of the famous residences in western Sichuan. It is paved with small green tiles and combined with modern technology to construct a unique Dayi Agricultural Science Base Exhibition Center (Figure 8).

In Chengdu, there is a subtropical humid monsoon climate zone. The days are short throughout the year, and the weather is hot and humid. Chengdu is known as "Rainy City". According to

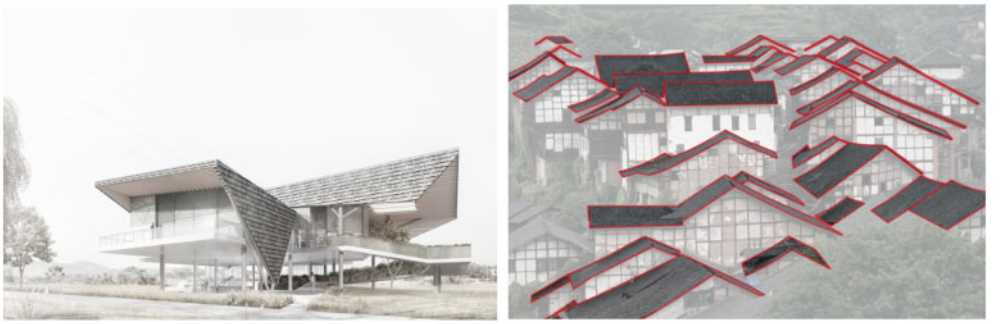

Figure 8. Dayi Agricultural Science Base Exhibition Center (picture source network).

climate conditions and functional requirements, the ancient historical period in Chengdu used a traditional architectural style of western Sichuan: dry-column construction (Figure 9).

Figure 9. Dry-column buildings (source: network).

3.3.2 *Ventilation and eco-design applications*

To inherit the national culture, the building of the exhibition center continues with the biggest feature of traditional buildings in western Sichuan: the ground floor is overhead, and its architectural shape is square, in the form of a "thousand-footed house," inheriting the "top to avoid heat and the bottom to avoid moisture" (Song 2020). This type of building increases the flow between the building and the natural wind, acts as thermal and moisture insulation, and can isolate the pests on the ground.

The overall volume of the building is lifted, and the vast space on the first floor becomes the activity space for wind and people. The open space is used for public resting seats and for planting and greening, which fully depicts the effectiveness of the space. The microclimate of the building is further adjusted by utilizing the transpiration of plants. In terms of materials, the exterior of the building is composed of glass curtain walls and steel structure rods, and large glass windows are installed. There are openings on the windward and the windward. There are no obstacles between the indoor openings and the air can flow smoothly. The formation of ventilation is beneficial to the air circulation and lighting inside and outside the building and effectively relieves indoor humidity (see Figure 10).

4 REALIZATION OF NATURAL VENTILATION IN BUILDINGS

Natural ventilation is an important factor affecting the building's design. The benefits of natural ventilation on the building are affected by factors such as structure dislocation, front-to-back

Figure 10. Void spaces of buildings (source: network).

relationship, location direction, size and number of windows, and material. The space layout should be carefully planned. However, in design, it is necessary to fully combine the local natural climate, environmental conditions, human history, economic conditions, and more, as well as formulate technical measures in line with regional characteristics to ensure natural ventilation with good ecological benefits and can be regarded as a real design.

4.1 *Chengdu dayi agricultural science base exhibition center*

The opening and closing of windows in buildings requires a rigorous knowledge of doors. In Feng Shui, the shape and orientation of windows are related to the five elements. If used properly, it will help strengthen the energy absorption of indoor space. Natural ventilation depends on the location, size, and shape of the windows in the building. The position of the opening affects the distribution of natural wind. The size of the cornice, the method of opening, and the use of materials in the window structure have different impact on the natural wind. Generally, the ventilation is used as the basic air circulation method, but the design aspects of the building should be respected and specific problems should be analyzed in detail with regard to whether it is suitable for the use of hall ventilation (Figure 11).

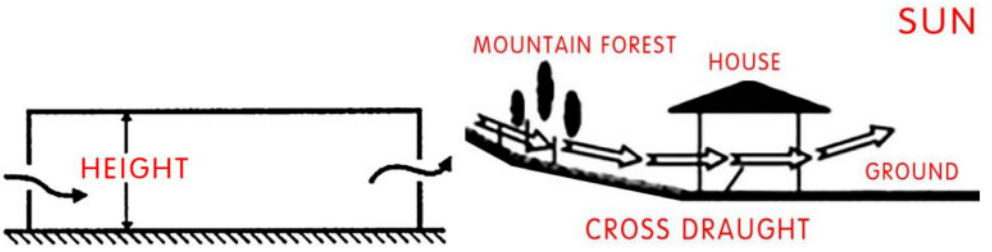

Figure 11. Schematic diagram of the ventilation in the hall (source: network).

4.2 *Realization of natural ventilation in building facades*

Reasonable building layout is one of the important ways in achieving natural ventilation. When designing the building scheme, the orientation of the building group and the structure between the buildings should be considered. Different structural composition methods have different blocking factors for wind force. Generally, the “bridge-connected” building composition method is adopted

to ensure that the building does not block the circulation of natural wind and reduce the building's pressure.

The building layout can be combined with large spaces, such as atriums and stairwells, to adjust the indoor air. For example, the Villa Savoye, designed by Le Corbusier, and the dry-style buildings at the Hemudu site in Yuyao all adopt the form of building facades on the ground floor. This structure is both artistic and practical and can effectively promote natural wind flow (Figure 12).

(a) The Villa Savoy (b) Schematic diagram of a dry building

Figure 12. (source: network).

In addition, in the atrium space of a large building, the vertical air density difference should be considered to design the atrium ventilation of the building. For example, the Qunxingcheng shopping mall in this article mainly strengthens the air circulation through the difference in densities between the high-temperature air and the low-temperature air. The air temperature in the atrium or the airshaft is higher. The small airflow tends to increase, and the air with a lower ambient temperature tends to decline due to high density, thus forming an up and down air circulation, which is the so-called atrium wind (Figure 13).

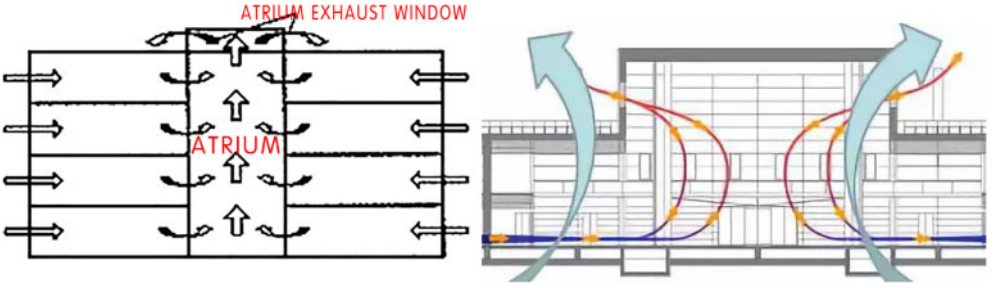

Figure 13. Ventilation in atrium building (source: network).

4.3 *The Realization of natural ventilation in other aspects of the building*

Natural ventilation is one of the key components of building ventilation. The roof is not only used as the top of the building, which acts as a thermal insulation and rain shelter, but can also be used as an independent part to promote natural ventilation of the building. For example, setting up lighting and ventilation, skylights, and roof insulation are the most common methods in modern technology. When the building cannot make use of the natural wind, some special materials can be comprehensively considered for realization of energy-saving ventilation, such as double-layer glass curtain walls, perforated metal plates, perforated aluminum plates, etc., as shown in Figure 14.

Figure 14. Ventilation material (source: network).

5 CONCLUSIONS

Urbanization has resulted in an increase in the number of high-rise buildings. However, some architects use the construction of high-rise buildings to develop their art and skills, continually destroying the original appearance of a city that is both unconventional and eye-catching (Wang et al. 2021). As a result, the relationship between the ecological benefit and the spatial environment of the building is gradually ignored. Based on this background, it is particularly important to trace the origin and study the relationship between architecture, nature, and people.

The development of the digital age has brought about many technologies to achieve ecological benefits, and there are many methods and means to implement ecological buildings. However, while natural ventilation is beneficial to human health, it also focuses on the concept of "energy-saving and environmental protection" and other ecological technologies. In contrast, natural ventilation is a low-cost and relatively mature technical system that helps save energy with fewer labor and materials. Natural ventilation systems play an essential role in energy savings and environmental protection in buildings, and are long-lasting.

To attain a more effective design, it is necessary to comprehensively consider the regional features of a building, its surroundings, and its own characteristics, as well as adapt design strategies appropriate to the actual design requirements. We must exhibit respect for nature to optimize the performance of natural ventilation in architectural design so that regional environmental belts can be alleviated. Natural ventilation serves the needs of people, allowing them to live in harmony with nature.

REFERENCES

Chen Jing, Ye Xin. Research on natural ventilation mode of Hong Kong public buildings [J]. Interior Design and Decoration, 2021(02): 118–119.

Li Min, Yang Zugui. Discussion on natural ventilation design in ecological architecture [J]. Sichuan Architecture, 2006(04): 29–30.

Song Zuomei. Architectural design of dry-column dwellings [J]. Industrial Architecture, 2020, 50(12): 230.

Wang Hui. Review and prospect of China's ecological civilization construction since the 18th National Congress of the Communist Party [J]. Comparative Research on Cultural Innovation, 2020, 4(12): 136–137.

Wang Yang, Chen Yongwen, Xu Ke. Research on the regional design mode of contemporary high-rise building complexes [J]. Architecture and Chemistry, 2021(05): 249–251.

Wang Zijia. Analysis of Building Energy Efficient Ventilation Design [J]. China Building Metal Structure, 2020(12): 86–87.

Xie Xiaolu, Ruan Guoshi. The modern translation of the architectural style characteristics of traditional residential houses in western Sichuan—the exhibition center of Dayi agricultural science base [J]. Architecture and Culture, 2020(04): 261–262.

Frontiers of Civil Engineering and Disaster Prevention and Control – Yang & Rahman (Eds)
© 2023 The Author(s), ISBN: 978-1-032-31200-2

Interaction between double-track tunnels when slurry shield passes through water-rich sand layer

Yilei Zhang & Jianxun Ma*
School of Human Settlements and Civil Engineering, Xi'an Jiaotong University, Xian, China

ABSTRACT: Taking the phase III project of Xi'an Metro Line 1 as the research background, the finite element model of single-track tunnel construction and double-track tunnel construction at the same time is established, and the relationship between the vertical displacement of soil and segment and the internal force of segment is obtained. The results show that: 1) when the double-track tunnel is constructed at the same time, the maximum vertical displacement of soil and segments is less than that of the single-track tunnel; 2) when the double-track tunnel is constructed at the same time, the internal force of the segment is greater than that of the single-track tunnel.

1 INTRODUCTION

The main features of slurry balance shield construction are that a diaphragm is set behind the cutterhead at the front end of the shield, a slurry pressure tank is formed between the cutterhead and the diaphragm, and the pressurized slurry is pumped to the slurry tank. When the mud tank is filled with mud at a certain pressure, a mud film will be formed on the excavation surface. The pressure of the mud tank acts on the soil on the excavation surface through the mud film, so as to maintain the stability of the excavation surface. Mud film formation and shield tunneling form a dynamic balance process. The cutterhead installed on the front of the shield rotates continuously to cut the soil containing mud film, and the mud film will be quickly formed on the new excavation surface. After the soil cut by the cutterhead is mixed with the mud water in the mud sump, it will be stirred by the mixing device to form a high-concentration mud water that will be transported to the ground by the mud pump and mud discharge pipeline.

Whether in the excavation stage or segment assembly stage, there is always a layer of mud film in order to ensure the stability of the excavation surface. When the mud film is cut by the cutter head, a new mud film will be formed rapidly and repeated again and again, so as to achieve the effect of maintaining the stability of the excavation surface. The mud film has good support effect on the excavation surface and little impact on the environment, which makes the mud water balance shield show strong vitality in various tunnel construction methods. At present, the research methods for shield construction stability mainly include the following: theoretical calculation method, numerical simulation method, and indoor model test method.

Theoretical calculation methods mainly include the limit analysis method and the limit equilibrium method. The limit analysis method is based on the upper and lower limit theorems of the extreme value theorem, also known as the upper and lower limit solution. The key to finding the upper bound solution is to determine the velocity field, including the assumed sliding surface. Usually, the surface passing through a point is selected as the possible sliding surface to obtain the approximate solution of the surface failure mode (Murakami 1995). The key to solving the lower bound solution is to build a stress field that includes the assumed sliding surface in order to stabilize the soil. The required ultimate load can be obtained directly by using the stress field. The limit equilibrium method considers that the failure of soil occurs on the sliding surface, and the soil meets the

*Corresponding Author

 DOI 10.1201/9781003308577-4

yield condition along the sliding surface. Assuming that the form of the sliding surface is known, such as a plane, circular arc surface, logarithmic spiral surface, or other irregular surfaces, the ultimate load or safety factor when the soil along the sliding surface is in the limit state is determined by considering the static balance and moment balance of each isolator in the sliding body.

The numerical simulation method has been widely used in shield construction. Wang Minqiang et al. (Wang & Chen 2002) used three-dimensional nonlinear finite elements to simulate the shield propulsion process and proposed a calculation model that can be used to investigate excavation surface stability. Xu Ming (Xu et al. 2012) did a three-dimensional numerical analysis on the stability of the excavation surface of the super large diameter shield in the sandy soil layer, focusing on the instability mode and ultimate support pressure of the excavation surface under different friction angles, and revealed the importance of the uneven distribution of support pressure caused by the unit weight of mud and water for the prediction results.

The indoor model test method is a research method carried out in the laboratory by reducing the actual project according to a certain proportion. It can more truly restore the actual situation of the site and predict the possible problems on the site in advance.

Taking the phase III project of Xi'an Metro Line 1 as the research object, this paper establishes a finite element model through Midas GTS NX to study the variation law of vertical displacement and internal force of soil and segments during the construction of single-track tunnels and double-track tunnels.

2 ENGINEERING BACKGROUND

The project is located in the middle of the alluvial plain of the Weihe River. The line crosses the floodplain of the Weihe River between the first and second stage areas. The Weihe River is a perennially flowing river. The water volume is greatly affected by seasonality. It is the largest tributary of the Yellow River. The geological conditions are mainly sandy soil with strong permeability. During shield construction, the diameter of the cutterhead is 6.28 m, the diameter of the segment is 6 m, and the length is 1.5 m. Every two segments are a construction step, and the buried depth of the tunnel is about 29 m.

3 FINITE ELEMENT SIMULATION

The finite element model consistent with the actual construction is established by using Midas GTS NX software. The length, width, and height of the soil in the model are 426 m, 81 m, and 75 m, respectively, to ensure the accuracy of the results. According to the geological survey report, the soil layers are miscellaneous fill, loess, sandy soil, and silty clay from top to bottom. The modified Moore-Coulomb model is adopted. See Table 1 for specific parameters. The shield shell is made

Table 1. Soil parameters.

Soil name	Poisson's ratio	Bulk density (g/cm^3)	Elastic modulus (MPa)	Cohesion (kPa)	Friction angle (°)	Dry density (g/cm^3)
Loess	0.30	1.85	8.70	33.00	25.30	1.53
Medium sand 1	0.35	2.20	30.00	0.00	34.50	1.77
Silty clay 1	0.30	2.00	7.00	30.80	18.20	1.64
Medium sand 2	0.25	2.00	30.00	5.60	32.87	1.74
Silty clay 2	0.29	2.02	7.00	47.00	27.30	1.67
Fine sand	0.28	2.00	20.00	0.00	30.48	1.74
Artificial fill	0.33	1.90	8.00	33.00	25.30	1.53

of Q345 steel, the segment and grouting layer are made of C50 concrete, the top surface of the model is a free surface, the bottom surface is a fixed surface, the normal displacement is restrained, and the water depth is set to 5 m. The activation and passivation of soil and segment are used to simulate the dynamic construction. The finite element model is shown in Figure 1.

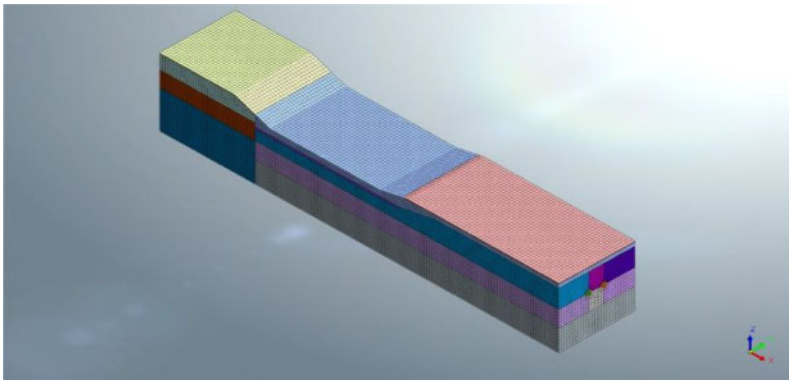

Figure 1. Finite element model.

4 NUMERICAL SIMULATION RESULTS

4.1 *Model reliability verification*

In order to verify the reliability of the finite element model, 8 points are taken every 3 m from the tunnel axis to both sides, and the displacement results are compared with the calculation results of Peck formula, as shown in Figure 2.

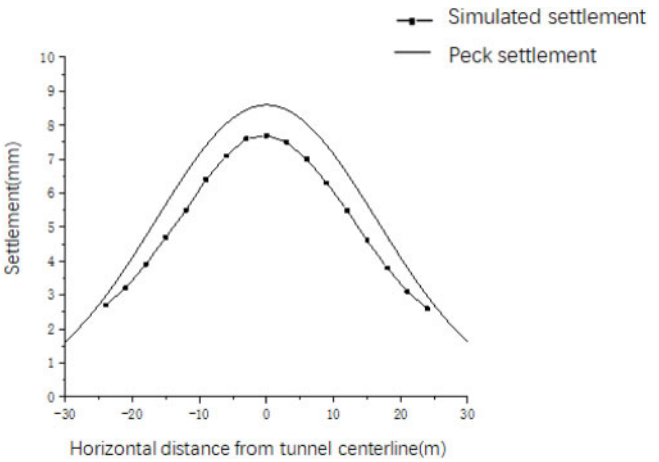

Figure 2. Comparison between numerical simulation results and calculation results.

As can be seen from the above figure, the simulation results and calculation results show a normal distribution, and the difference between the values is very small, which can verify the reliability of the model.

4.2 *Influence of double-track tunnel construction on vertical displacement of soil and segments*

In the process of shield construction, the vertical displacement of soil and segments during the simultaneous construction of two tunnels is different from that of a single tunnel. It is of great significance to study the interaction of double-track tunnels to select appropriate construction parameters to guide the construction.

Take a node every 30m on the model as the research object, and compare the change of vertical displacement during the construction of a single-track tunnel and a double-track tunnel at the same time. The change of soil vertical displacement is shown in Figure 3, and the change of segment vertical displacement is shown in Figure 4. It can be seen that the maximum vertical displacement of soil and segments during the construction of a double-track tunnel is less than that of a single-track tunnel.

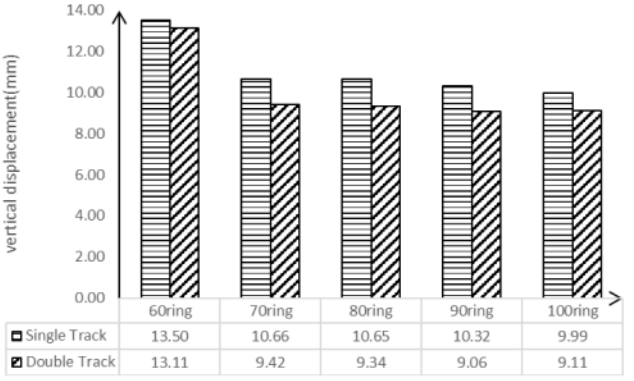

Figure 3. Relationship between the number of tunnels and the vertical displacement of soil mass.

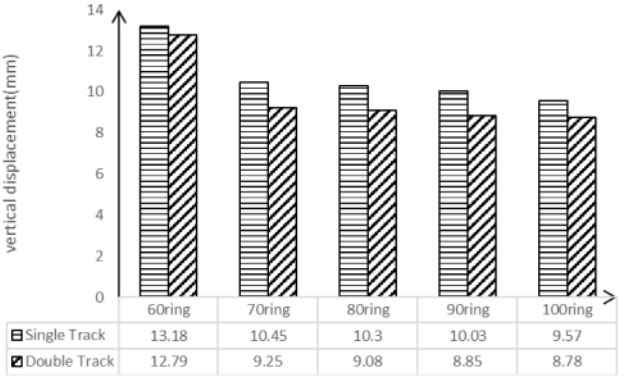

Figure 4. Relationship between the number of tunnels and the vertical displacement of segments.

4.3 *Influence of double-track tunnel construction on segment internal force*

Take segments every 30 m on the model, and take the segment apex as the research object to analyze the changes in internal force during single-track construction and double-track construction. The results are shown in Figure 5. It can be seen from the figure that the internal force of the segment during the construction of a double-track tunnel is greater than that of a single-track tunnel.

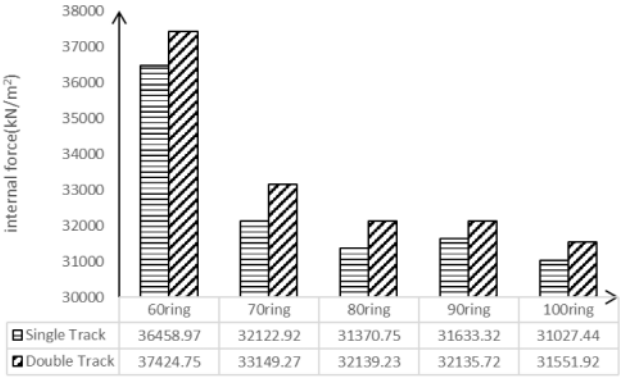

Figure 5. Relationship between the number of tunnels and segment internal force.

4.4 *Comparison between numerical simulation results and field monitoring data*

The statistics of the numerical simulation results of riverbed settlement are shown in Figure 6, and the field monitoring data are shown in Table 2.

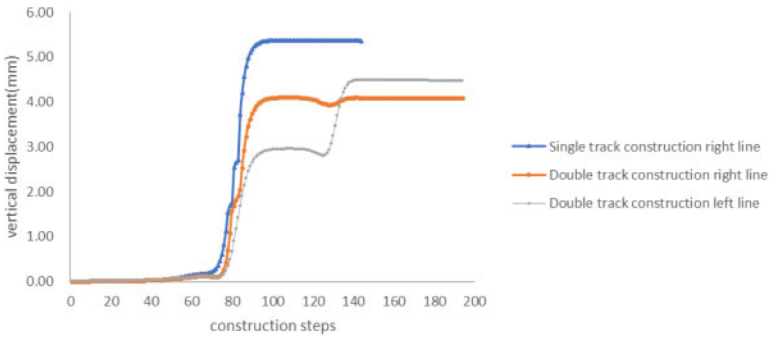

Figure 6. Riverbed settlement value.

Table 2. Settlement value of monitoring results.

	Monitoring point	Settlement value (mm)
Right line	2	4.87
	4	5.00
	6	5.40
	8	1.68
	10	3.95
	12	3.67
Left line	1	4.84
	3	3.10
	5	1.46
	7	2.37
	90	1.95
	11	4.38

The monitoring data shows that the maximum settlement value of the riverbed above the tunnel during single-track construction is about 5 mm. During double-track construction, the maximum settlement value of the right line is about 4 mm and the maximum settlement value of the left line is about 4.5 mm, which is consistent with the simulation results.

5 CONCLUSIONS

In this paper, a finite element model consistent with the actual project is established by Midas GTS NX to study the vertical displacement of soil and segments and the change of segment internal force during the construction of single-track tunnels and double-track tunnels when the slurry shield passes through the water-rich sand layer. The conclusions are as follows:

(1) During the construction of a double-track tunnel, the maximum vertical displacement of soil and segments is less than that of a single-track tunnel.
(2) During the construction of a double-track tunnel, the internal force of each segment is greater than that of a single-track tunnel.

6 OUTLOOK

This paper mainly studies the influence of a double-track tunnel on the vertical displacement of soil and segment and the internal force of the segment when a slurry shield passes through a water-rich sand layer. There are still some problems that can be further improved in the follow-up research:

(1) In the highly permeable stratum, the seepage force of water will have a certain impact on the results. For technical and time reasons, the seepage effect is not considered in this paper. In future research, the seepage conditions can be added to the finite element model for analysis.
(2) Surface settlement is influenced by the hardening time of the grouting layer. In this paper, we focus only on the onset and completion of hardening, and future research can be conducted to examine the hardening time of the grouting layer.

REFERENCES

M H, Murakami E. Stability and failure mechanisms of a tunnel face with a shallow depth: proceedings of the Proceedings of the 8th Congress of the International Society for Rock Mechanics, F, 1995 [C]. International Society for Rock Mechanics.

Wang Minqiang, Chen Shenghong. Three-dimensional nonlinear finite element simulation of shield driven tunnel structure [J]. Journal of rock mechanics and engineering, 2002(02): 228–232.

Xu Ming, Zou Wenhao, Liu Yao. Stability analysis of excavation face of super large diameter slurry shield in sand [J]. Journal of civil engineering, 2012, 45(03).

Frontiers of Civil Engineering and Disaster Prevention and Control – Yang & Rahman (Eds)

Seismic reliability analysis of pipeline in underground powerhouse of Baihetan hydropower station

Jie Fang* & Shengbing Li
Huadong Engineering Corporation Limited, Hangzhou, Zhejiang, China

Baoshan Zhu, Zhigang Zuo & Shuhong Liu
State Key Laboratory of Hydro Science and Engineering, Department of Energy and Power Engineering, Tsinghua University, Beijing, China

Chunjian Cao
Huadong Engineering Corporation Limited, Hangzhou, Zhejiang, China

ABSTRACT: In this paper, a simplified calculation model of the underground workshop pipeline system has been established to study the seismic reliability of the pipeline system in the underground powerhouse of Baihetan Hydropower Station. The structural dimensions and material properties of the pipeline and bracket pillar are treated as random variables with a Gaussian distribution. A pipeline sampling method is used to analyze the pipeline system. The seismic reliability of the pipeline system under actual conditions has been proven. Sensitivity analysis shows that the material density and elastic modulus of the pipeline are the most important factors affecting the seismic reliability of the pipeline system. This study provides theoretical support for seismic reliability and structural optimization for similar pipeline systems.

1 INTRODUCTION

Baihetan Hydropower Station is located in Ningnan County, Sichuan Province and Qiaojia County, Yunnan Province in the lower reaches of the Jinsha River. It is the second-stage hydropower station for cascade development in the lower reaches of the Jinsha River, with Wudongde Hydropower Station in the upper part and Xiluodu Hydropower Station in the lower part. The controlled basin area is 430,300 km^2, accounting for 91.0% of the Jinsha River basin area. The main tasks of power station development are to generate electricity, consider flood control and shipping, and promote local economic and social development (Dai et al. 2006; Fan et al. 2019; Ma et al. 2020). Because the hydropower station is located in an earthquake-prone area of China, it is particularly important to analyze the seismic reliability of each pipeline system in the underground powerhouse of the hydropower station. Many papers (Ai & Li 2007; Dong et al. 2008; Gazis & Nikolaos 2011; Han & Jame, 2014; Wang & Hong 1993; Wang et al. 2005, 2019; Zhang et al. 2010) have studied the dynamic characteristics and seismic response of submarine pipelines and buried pipelines based on numerical or experimental methods. Chen (Chen 1996) has studied the reliability of above-ground pipelines under earthquakes. However, the research on the reliability of the above-ground suspended pipeline under an earthquake is rarely seen in the open literature. Based on this, this paper adopts the PDS module in ANSYS finite element software, which is widely used to preliminarily study the safety and reliability of the suspended pipeline of the underground powerhouse of Baihetan Hydropower Station under an earthquake.

The ANSYS-PDS module combines finite element technology and probability design theory (Ye et al. 2004; Qin 2006). By setting random variables that conform to certain distribution rules as

*Corresponding Author: fang_j@hdec.com

 DOI 10.1201/9781003308577-5

input parameters, after limited cycle sampling, it cannot only get more accurate failure probability values to evaluate customers' design satisfaction with product quality and reliability, but also get the sensitivity analysis results of each input parameter to output parameters, so as to properly adjust and control each input parameter according to the sensitivity degree, and achieve the purpose of improving product safety and reliability. He Shuanghua et al. (2012) applied the ANSYS-PDS module to earthquake damage prediction models and random reliability analyses of underground pipelines, which provided a scientific basis for optimization of underground pipelines. Li Wenzhen et al. (Li et al. 2018) used the ANSYS-PDS function to analyze the reliability of a pressure vessel and obtained the sensitivity of design parameters such as stress probability distribution characteristics, pressure load, and wall thickness to stress distribution. Zhu Yuankun and others (Zhu et al. 2017) applied the ANSYS-PDS module to analyze the reliability of the tubing hanger structure, which provided theoretical support for the reliability and structural optimization of other underwater complex structures such as the tubing hanger. Zhang Aihua et al. (Zhang & Ren 2010) applied ANSYS-PDS module design to analyze the anti-resonance reliability of a high-speed motorized spindle. Rong Zhixiang and others (Rong & Lin 2011) applied the ANSYS-PDS module to analyze the reliability of the connecting rod.

In this paper, the reliability of suspended pipeline systems under earthquakes is mainly analyzed, and the reliability analysis model under normal service limit state is established. Through the Monte Carlo method and Latin Hypercube Sampling technology (Gao et al. 2008; Wang et al. 2006; Zhao et al. 2015), the related design parameters of the pipeline system (pipeline and support column) are randomly sampled, and the seismic reliability analysis of the pipeline system is completed on the basis of finite element analysis.

2 NUMERICAL ANALYSIS METHOD AND SIMULATION MODEL

2.1 *Reliability related theory*

The reliability of the structure refers to the probability that the structure will complete the predetermined function within the specified time and under the specified conditions (normal service limit state and bearing capacity limit state) (Li & Zhou 2001; Pan 2005; Wu 2009; Yu et al. 2017, 2016, 2008; Yan et al. 2007).

The basic variables of the structure consist of X1, X2, ..., Xn, and the structural function Z is a function of the basic variables, then the functional function (limit state function) of the structure can be expressed as:

$$Z = g(X_1, X_2, \cdots X_n) \tag{1}$$

In the probabilistic limit state design theory, the limit state equation is:

$$g(X_1, X_2, \cdots X_n) = 0 \tag{2}$$

Therefore, in the structural design of probability limit state, the following conditions must be met:

$$Z = g(R, S) = R - S \geq 0 \tag{3}$$

According to the reliability theory, the reliability of a structure is the probability of the limit state function $g(X_1, X_2, \cdots X_n) \geq 0$, so the reliability of the structure can be obtained by using ANSYS probability analysis of the probability calculated by PDS module function.

2.2 *Case overview*

Select a section of pipeline in the turbine layer of Baihetan underground powerhouse, with a length of L = 12.525 m. Poisson's ratio γ of pipe material is 0.3; Poisson's ratio γ of support column material is 0.3; initial thickness r of pipe wall is r = 5 mm; pipe material is stainless steel; yield strength is 205 Mpa; support column material is ordinary carbon steel Q235; and yield strength is 235 MPa.

2.3 *Finite element analysis model*

In the ANSYS finite element model of the pipeline system, the pipeline and the support column are set as rigid connections. All the models adopt Beam188 beam elements, and parametric modeling is carried out by Ansys Parametric Design Language (APDL). The model building process is as follows:

- The displacement constraints, i.e., UX=0, UY=0 and UZ=0, are imposed on the nodes of X =-75 $\sim$ 0, Y = 0 and Z = 0;
- The displacement constraints, i.e., UX=0, UY=0 and UZ=0, are imposed on the nodes with X =-75 $\sim$ 0, Y=4500$\sim$4575 and Z = 0;
- The displacement constraints, i.e., UX=0, UY=0 and UZ=0, are imposed on the nodes with X =-75 $\sim$ 0, Y=7850$\sim$7925 and Z = 0;

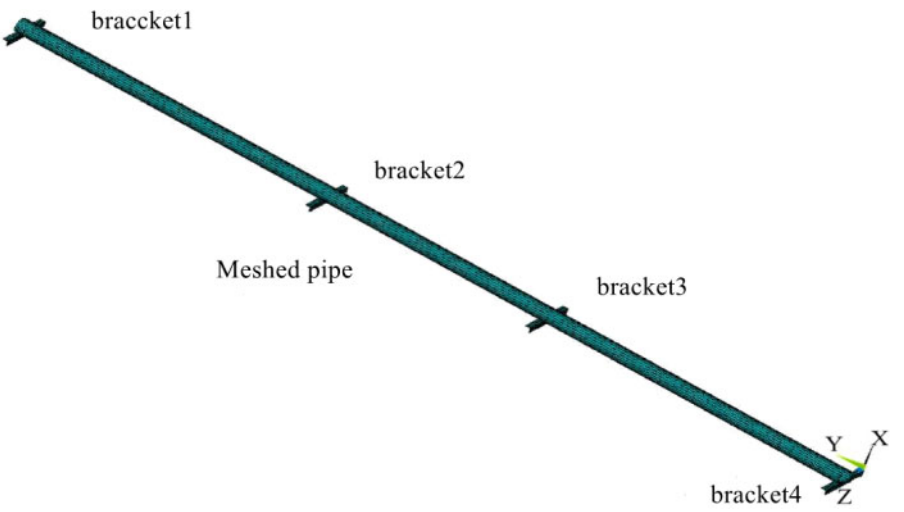

Figure 1. Finite element modeling with ANSYS.

- The displacement constraints, i.e., UX=0, UY=0 and UZ=0, are imposed on the nodes with X =-75 $\sim$ 0, Y=12450$\sim$12525 and Z = 0;
- The displacement constraints, i.e., UX=0 and UZ=0, are applied to the nodes with X = 110 $\sim$ 220, Y=25 and Z=340$\sim$560;
- The displacement constraints, i.e., UX=0 and UY=0, are imposed on the nodes with x = 0 $\sim$ 110, Y=4525 and Z=340$\sim$560;
- A displacement constraint, i.e., UX=0, is imposed on the nodes with X = 0 $\sim$ 110, Y=7875 and Z=340$\sim$560;
- The displacement constraints, i.e., UX=0 and UZ=0, are applied on the nodes with X=110$\sim$220, Y=12475, Z=340$\sim$560.

Finally, the three-dimensional finite element model of simplified pipes and supports is established, as shown in Figure 1.

2.4 *Variable setting for seismic reliability calculation of pipeline system*

In reality, there are randomness such as processing size errors and $Z1 = DS - UMAX \geq 0$ material parameters of pipes and support columns, which obey certain distribution. Therefore, in this paper, only 11 parameters of the sizes and material parameters of pipes and support columns are selected as

random variables. See Table 1 for the random variable parameters and their distribution characteristics of the selected pipe and support column materials. Enter the PDS analysis module of ANSYS software, specify the completed reliability analysis documents, and define the random input variables, the output variables of the limit displacement failure state function $Z1 = DS - UMAX \geq 0$ and the output variables of the limit strength failure state function $Z1 = DS - UMAX \geq 0$.

Table 1. Distribution of random input variables for pipeline and bracket pillar parameters.

Random variable name	Parameter meaning	Distribution pattern	Average/mean value	Standard deviation
W1	Column section length	Normal distribution	75 mm	2 mm
W2	Column section length	Normal distribution	75 mm	3 mm
T1	Column section width	Normal distribution	8 mm	0.2 mm
T2	Column section width	Normal distribution	8 mm	0.35 mm
RT	Inner diameter of pipe	Normal distribution	105 mm	1 mm
YOUNG1	Elastic modulus of column	Normal distribution	2.06E5 N/mm^2	2.06E3 N/mm^2
YOUNG2	Elastic modulus of pipeline	Normal distribution	1.95E5 N/mm^2	1.95E3 N/mm^2
DENSITY1	Column density	Normal distribution	7.8E-9 t/mm^3	1E-10 t/mm^3
DENSITY2	Pipeline density	Normal distribution	7.9E-9 t/mm^3	1E-10 t/mm^3
DS	Pipeline failure check displacement	Normal distribution	11 mm	0.5 mm
CH	Pipeline failure checking strength	Normal distribution	164 Mpa	12 Mpa

2.5 *Seismic reliability analysis of pipeline system*

The TH4TG045 synthetic seismic wave has been selected, and its peak acceleration is 2,048 mm/s^2 at 2.6 s over the duration of an action lasting 10 seconds. The Monte Carlo method (Monte Carlo method) and Latin Hypercube Sampling (U-IS sampling method) were used to randomly sample the geometric finite element models of pipes and support columns, and the sampling times were 500 times, and the sampling trends of the ultimate displacement failure state function Z1 and the ultimate strength failure state function Z2 shown in Figure 2 were obtained. Among the three sampling curves, the upper and lower curves represent the upper and lower limits of the confidence interval, and the middle curve represents the change of the sampling mean.

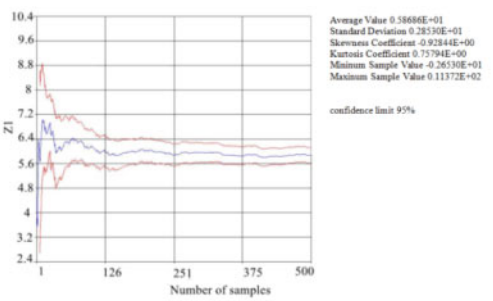

(a) Sampling curve of limit displacement failure state function Z1

(b) Sampling curve of ultimate strength failure state function Z2

Figure 2. Sampling result curve.

As can be seen from Figure 2, the three curves tend to be horizontal in the later stages, and the average values of the sampling curves of limit displacement failure state function Z1 and limit

strength failure state function Z2 gradually converge, which indicates that 500 sampling times can meet the accuracy requirements of reliability analysis of pipelines and support columns. In order to verify whether the sampling times of the probability analysis (PDS) simulation results are enough, the histogram of random variables can be drawn as a reference. Because there are many random input variables, only the distribution histograms of random variables W1 and YOUNG2 are given in Figure 3.

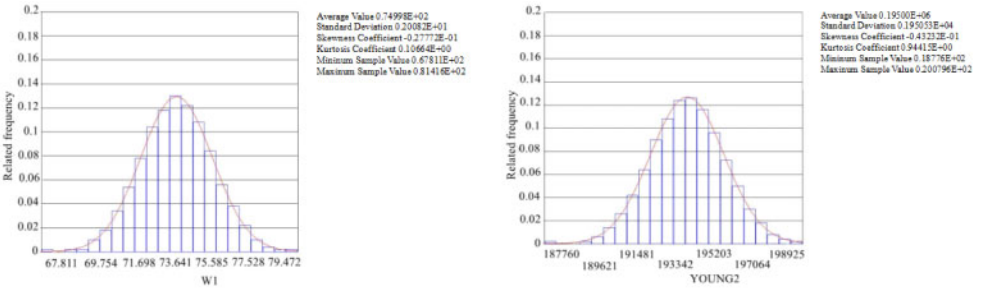

(a) Input variable of section length of support column

(b) Input variable of pipeline elastic modulus

Figure 3. Random input variable histogram.

It can be seen from Figure 3 that the distribution histograms of W1 and YOUNG2 are close to the normal distribution curve, and the curve is smooth, which shows that the sampling times are enough to ensure the accuracy of the analysis results.

3 NUMERICAL CALCULATION RESULTS AND DISCUSSION

3.1 *Seismic reliability analysis results of pipeline system*

List probability (possibility): PDS provides a function using the command PDPROB to determine the value of any point of the cumulative distribution function on the axis of probability design variable, including interpolation function, so that the data between sample points can be evaluated. This property is very effective for evaluating the failure probability of structures at given data. The results show that the probability of $Z1<0$ and $Z2<0$ is 0.05872 and 0, respectively, when the confidence level of this pipeline system is 95%, and the reliability of these two failure state functions is 94.128% and 100%, as shown in Figure 4 and Figure 5.

3.2 *Sensitivity analysis results*

Sensitivity analysis is an important part of probability analysis in the ANSYS-PDS module. Figure 6 shows the results of sensitivity analysis for the ultimate displacement failure state function Z1 and the ultimate strength failure state function Z2 for the pipeline system under the influence of seismic waves.

As can be seen from Figure 6, the main factors that have significant influence on the ultimate displacement failure function Z1 are the material density, elastic modulus, and check displacement of the pipeline, and the input variables for the material density and check displacement of the pipeline are positive (the positive sign indicates that the change of this random variable has a positive effect on the structural reliability), which indicates that the reliability of the system increases with the increase of this random variable. The elastic modulus of the pipeline is negative (the negative sign indicates that the change of this random variable has a negative effect on the structural reliability), indicating that the reliability of the system decreases with the increase of the change. The main

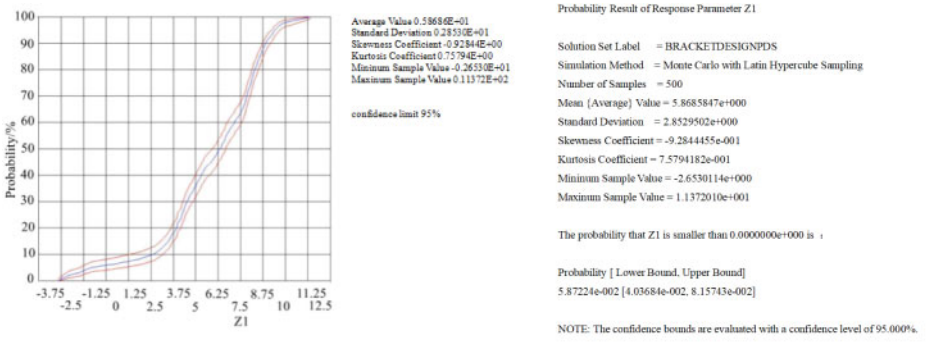

(a) Cumulative distribution function of limit displacement failure state function Z1

(b) Probability of failure state function Z1 of limit displacement

Figure 4. Reliability analysis results of ultimate displacement failure state function Z1.

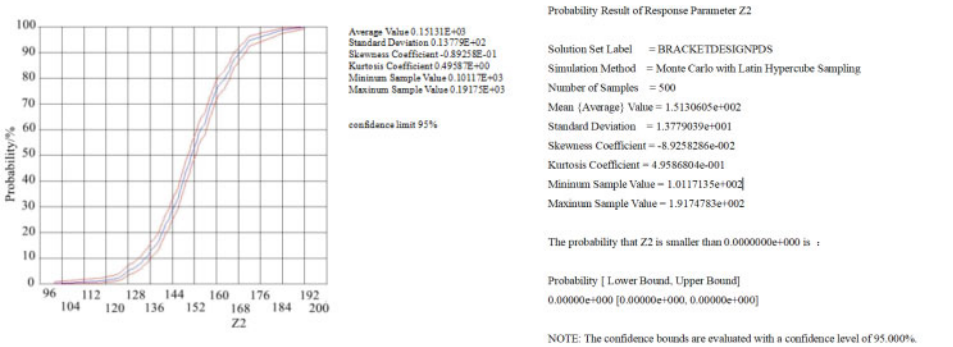

(a) cumulative distribution function of ultimate strength failure state function Z2

(b) Probability of failure state function Z2 of ultimate strength

Figure 5. Reliability analysis results of ultimate strength failure state function Z2.

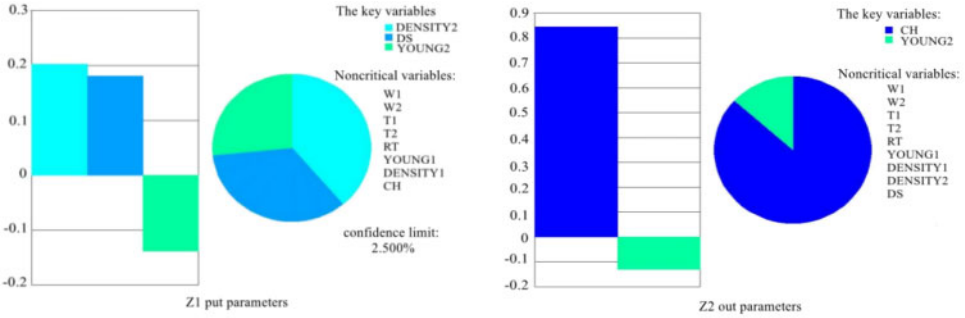

(a) Output parameters of the limit displacement failure state function Z1

(b) Output parameter of ultimate strength failure state function Z2

Figure 6. Sensitivity analysis results.

variables that have significant influence on the ultimate strength failure function Z2 are the elastic modulus and check stress of the pipeline, with the check stress input variable being positive, whereas the elastic modulus input variable of the pipeline is negative.

The influence degree of 11 random input variables selected on the reliability of the pipeline system is shown in Table 2 and Table 3. In order to ensure the structural reliability of the pipeline system, the related random design variables should be adjusted according to the results of sensitivity analysis. For example, the variables that have significant influence on reliability should be strictly controlled in the design and manufacturing process. In order to reduce the maximum displacement and the maximum stress of the pipeline system structure, the following measures should be taken first: optimize the structure size instead of considering other unimportant random design variables.

Table 2. Influence degree of random variables on reliability of ultimate displacement failure state function Z1 of pipeline system.

W1	W2	T1	T2	RT	
−0.058	0.011	−0.055	−0.043	−0.054	
YOUNG1	YOUNG2	DENSITY1	DENSITY2	DS	CH
−0.025	−0.139	0.069	0.203	0.181	−0.001

Table 3. Influence degree of random variables on reliability of ultimate strength failure state function Z2 of pipeline system.

W1	W2	T1	T2	RT	
−0.023	−0.038	0.003	0.033	−0.034	
YOUNG1	YOUNG2	DENSITY1	DENSITY2	DS	CH
0.001	−0.130	−0.006	0.094	0.061	0.845

4 CONCLUSIONS

In this paper, the APDL modeling-analysis command flow file of a pipeline system structure of the underground powerhouse of Baihetan Hydropower Station is compiled by using the ANSYS analysis platform, and the PDS analysis module is used to analyze the seismic reliability of the pipeline system structure. The main conclusions are as follows:

- It provides a simulation analysis method for seismic reliability analysis of pipeline system structure;
- The analysis results show that the limit displacement failure state function Z1 and the limit strength failure state function Z2 of the pipeline system are both highly reliable at 94.128% and 100%, respectively;
- Through sensitivity analysis, it can be seen that the elastic modulus, material density, and check displacement of the pipeline are the key factors affecting the structural reliability of the ultimate displacement of the pipeline system;
- The elastic modulus and check strength of the pipeline are the key factors that affect the structural reliability and ultimate strength of the pipeline system.

Through the numerical simulation analysis of a pipeline example in the hydraulic turbine layer of the underground powerhouse of Baihetan Hydropower Station, it is proved that it is feasible to use the ANSYS-PDS module function to analyze the failure probability or reliability of this pipeline

system, which provides a basis for the subsequent optimization design of other pipeline systems in the underground powerhouse of Baihetan Hydropower Station.

REFERENCES

Chen Huai. (1996) Seismic reliability analysis of above-ground pipelines. J. Industrial Architecture, 26(011): 24–27.

Dai Huichao, Cai Zhiguo, He Wenshe, et al. (2006) Review on the research and practice of cascade operation of cofferdam of Three Gorges-Gezhouba Water Control Project during power generation. J. Journal of Hydropower, 25(6): 8–15.

Dong Rubo, James Zhou, Feng Xin. (2008) Seismic response analysis of partially suspended submarine pipeline under multi-input. J. Journal of Vibration Engineering, 21(2):146–151.

Fan Qixiang, Zhang Chaoran, Chen Wenbin, et al. (2019) Key technologies of intelligent construction of ultra-high arch dams in Wudongde and Baihetan. J. Journal of Hydropower, 38(2): 22–35.

Gao Juan, Luo Qifeng, Che Wei. (2008) Monte Carlo theory and its realization in ANSYS. J. Journal of Qingdao University of Technology, 29(004): 18–22.

GAZIS, NIKOLAOS. (2011) Monte Carlo-based response analysis of subsea free spanning pipeline systems subjected to non-stationary random seismic excitations. Oceans'11 MTS/IEEE KONA.: IEEE, pp. 1–8.

Han Wenhai, James Zhou. (2014) Seismic reliability analysis of suspended span of corroded submarine pipeline. J. Chemical Equipment and Pipeline, 51(5): 75–78.

He Shuanghua, Song Can. (2012) Seismic damage prediction model and random reliability analysis of underground pipelines. Journal of North China Institute of Water Resources and Hydropower, 33(2): 4.

Li Dianqing, Zhou Jianfang. (2001) Back analysis method of reliability in mechanical design. J. Mechanical design, 18(3): 33–35.

Li Wenzhen, Huang Si, Xu Zhengnan. (2018) Reliability analysis of pressure vessel based on PDS module of ANSYS software. J. Machinery Manufacturing, 56(012): 14–16, 30.

Ma Bin, She Xin, Guo Yiliang. (2020) Experimental study on hydroelastic model of flood discharge and vibration reduction in Wudongde hydropower station. J. Journal of Hydropower, 39(1): 110–120.

Pan Xueguang. (2005) Causes and prevention of submarine pipeline suspension. J. China Ship Inspection, (10): 68–69.

Qin Quan. (2006) Stochastic finite element method of structural reliability: theory and engineering application. Tsinghua University Press, Beijing.

Rong Zhixiang, Lin Shaofen. (2011) Reliability analysis of connecting rod based on stochastic finite element method. J. Naval Science and Technology, 33(9): 68–70.

Wang Qianxin, Hong Feng. (1993) Seismic displacement response and seismic reliability analysis of offshore pipeline bridge. J. Earthquake Engineering and Engineering Vibration, 013(003): 43–53.

Wang Xiaoling, Li Xiao, Zhu Xiaobin, et al. (2019) Reliability analysis of dam foundation anti-sliding stability based on PLS-ELM response surface method. J. Journal of Hydropower, 38(4): 224–233.

Wang Yan, Yin Haili, Dou Zaixiang. (2006) Application of Monte Carlo Method. J. Journal of Qingdao University of Technology, 27(2): 111–113.

Wang Yuchuan, Zhao Changjun, Huang Gang, et al. (2014) Quantitative evaluation of failure probability of oil and gas pipelines with cracks. J. Safety and Environmental Engineering, 21(3): 126–129.

Wang Zhiping, Li Xia, Zhan Liu, et al. (2005) Reliability analysis and calculation of buried pipeline corrosion. J. Mechanical strength, 27(3): 339–341.

Wu Shiwei. (2009) Structural reliability analysis. People's Communications Press.

X.Q.AI, J.H.LI. (2007) Seismic reliability analysis of underground pipelines based on probability density evolution method. The first international symposium on geotechnical engineering safety and risk (proceedings of the first international symposium on geotechnical safety & risk is GSR 2007).

Yan Hongsheng, Yu Jianxing, Hu Yunchang, et al. (2007) Research on reliability analysis method of large-scale structural system. J. Ship Mechanics, 11(3): 444–452.

Ye Yong, Hao Yanhua, Zhang Changhan. (2004) Structural reliability analysis based on ANSYS. J. Mechanical Engineering and Automation, (6): 63–65.

Yu Jianxing, Fu Mingxi, Yang Yi, et al. (2008) Reliability analysis of vortex-induced vibration fatigue of submarine pipelines. J. Journal of Tianjin University, 41(11): 1321–1325.

Yu Jianxing, Guo Shuai, Yu Yang, et al. (2016) Influence of crack parameter on fatigue life of deep-water submarine pipeline. J. Journal of Tianjin University, 49(9): 889–895.

Yu Jianxing, Liu Xiaoqiang, Yu Yang, et al. (2017) Riser fatigue reliability calculation based on improved response surface method. J. Journal of Tianjin University, 50(10): 1011–1017.
Zhang Aihua, Ren Gongchang. (2010) Reliability analysis of anti-resonance of high-speed motorized spindle based on probability design of ANSYS. J. Mechanical Design and Manufacturing, 7: 112–114.
Zhang Lisong, Yan Xiangzhen, Xiujuan Yang. (2010) Application research of parameter reliability back analysis method in X80 steel pipeline design. J. Pressure Vessel, 27(8): 19–23.
Zhao Huigan, Guo Mingzhu, Zhai Changda, et al. (2015) Reliability analysis of seismic connectivity of urban gas pipeline network based on Monte Carlo method. J. Earthquake Research, 038(002): 292–296.
Zhu Yuankun, Liu Jian, Qin Haozhi, et al. (2017) Reliability analysis of tubing hanger structure based on ANSYS. J. Oil Field Machinery, 46(4): 28–31.

Frontiers of Civil Engineering and Disaster Prevention and Control – Yang & Rahman (Eds)
© 2023 The Author(s), ISBN: 978-1-032-31200-2

Study on the distribution law of sidewall earth pressure during the sinking stage of a super large open caisson

Zhewen Chen
School of Civil, Architectural and Environmental Engineering, Hubei University of Technology, Wuhan, China
State Key of Geomechanics and Geotechnical Engineering, Institute of Rock and Soil Mechanics, Chinese Academy of Science, Wuhan, China

Tiechui Yang
Power China Henan Electric Power Engineering Co. Ltd, Zhengzhou, Henan, China

Gaojie Lan
State Key of Geomechanics and Geotechnical Engineering, Institute of Rock and Soil Mechanics, Chinese Academy of Science,Wuhan, China
School of Civil Engineering and Architecture, Anhui University of Science and Technology, Huainan, China

Mingwei Guo*
School of Civil, Architectural and Environmental Engineering, Hubei University of Technology,Wuhan, China
State Key of Geomechanics and Geotechnical Engineering, Institute of Rock and Soil Mechanics, Chinese Academy of Science,Wuhan, China

ABSTRACT: Considering the open caisson of the Changtai Yangtze River Bridge project as the research object, based on the monitoring data of the sidewall soil pressure during the sinking process of the caisson foundation, the distribution characteristics of the sidewall soil pressure are analyzed. A new distribution model for the sidewall soil pressure was proposed in comparison with the existing distribution model. The analysis results show that the soil pressure of the sidewall increases linearly in a specific range with the sinking depth of the caisson and then decreases with the depth after reaching the peak, and finally remains constant. Furthermore, the location corresponding to the peak value of the sidewall soil pressure moves down with the increase in the sinking depth.

1 INTRODUCTION

The large caisson foundations are increasingly being used with the increasing construction of large bridge projects in China. It is critical for expanding research on the sinking of large caissons (Guo et al. 2021; Shi et al. 2019). It was found that with the increasing size of the caisson foundation, the proportion of side friction resistance decreases in the total resistance of caisson sinking, and the proportion of Changtai caisson is 0.37 (Qin et al. 2019). Zhou Hexiang et al. (2018) and Zhou, Ma, Zhang, et al. (2018) carried out centrifugal simulation experiments with the local models of straight-arm open caisson and stepped open caisson. They proposed the calculation model of sidewall friction resistance according to the experimental results of the centrifugal simulation experiments. Zhang Kai et al. (Zhang et al. 2019,) studied the sinking process of the caisson by centrifugal simulation experiments with the main pier of the Hutong Yangtze River Bridge. They concluded that the sidewall soil pressure of the caisson first increases and then decreases, and the sidewall soil pressure reaches extreme when the depth of entry is two-thirds of the final sinking depth. They proposed a calculation model of the sidewall soil pressure related to the frictional resistance. He Qiaoling et al. (He et al. 2020) monitored the sidewall earth pressure during the

*Corresponding Author: 562913072@qq.com

sinking of the south anchor caisson foundation of Taizhou Bridge in real time and analyzed the data to derive the distribution form of the frictional resistance. Jiang Bingnan et al. (Jiang et al. 2019) considering the construction process of Hutong Bridge-29 # caisson as their research object, monitored the whole construction process. Post eliminating the influence of tilt on the caisson, they derived the distribution form of sidewall earth pressure along the depth of the open caisson and proposed that the calculation model of sidewall earth pressure be used as the basis for the calculation of sidewall friction resistance.

Chen Xiaoping et al. (Chen et al. 2005) monitored the whole process of soil extraction and sinking of the main pier caisson of the Haikou Century Bridge and derived the calculation model of sidewall earth pressure based on the monitoring data obtained. However, at present, there is no uniform distribution model of sidewall soil pressure during the sinking process of a super large caisson foundation.

Based on the large caisson foundation of the Changtai Yangtze River project, this paper deeply analyzes the distribution characteristics of sidewall soil pressure based on the measured data during the sinking process of the open caisson. Furthermore, a new distribution model of the sidewall soil pressure was proposed based on the existing calculating model.

2 CHANGTAI YANGTZE RIVER BRIDGE PROJECT OVERVIEW

As seen from Figure 1, the caisson foundation of the main tower of the Changtai Changjiang River Bridge is in the form of a circular end-shaped plane. The sidewall earth pressure sensors are divided into six layers, as shown in Figure 2.

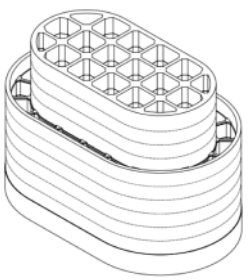

Figure 1. Elevation drawing of open caisson.

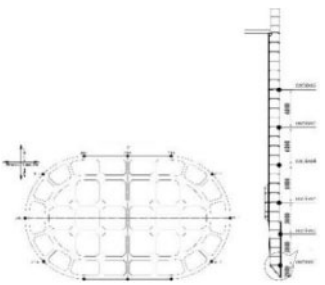

Figure 2. Monitoring point layout map.

The caisson foundation of the main pier is located in geological conditions with a sediment thickness higher than 170 m, as shown in Table 1.

Table 1. Open caisson stratigraphic parameters.

Soil layer	Top altitude (m)	Bottom altitude (m)	γ (kN/m^3)	c′ (kPa)	φ' (°)
Loose silty sand	−14.7	−17.0	2	2	29.5
Hard plastic silty clay	−17.0	−24.4	19.8	29.3	10.6
Loose silty sand	−24.4	−25.6	20.6	5.6	31.8
Hard plastic silty clay	−25.6	−27.7	19.8	29.3	10.6
Slightly dense fine sand	−27.7	−32.7	19.8	2.5	33.39
Silt silty clay	−32.7	−34.0	19	29.7	4.8
Medium dense silty sand	−34.0	−39.4	20.6	5.6	31.4
Medium dense fine sand	−39.4	−50.2	19.8	2.5	33.39

(*continued*)

Table 1. Continued.

Soil layer	Top altitude (m)	Bottom altitude (m)	γ (kN/m^3)	c′ (kPa)	φ' (°)
Soft plastic silty clay	−50.2	−51.3	19	27.8	7.2
Dense medium sand	−51.3	−54.2	20	2	34.47
Dense coarse sand	−54.2	−70.0	20.8	2	36.55

3 MONITORING DATA OF SIDEWALL SOIL PRESSURE

After floating the caisson into the target position, it was sunk with water injection, and sinking was carried out until the elevation of the outer edge of the caisson reached −26.8 m, finally reaching the sinking depth of −65 m. Because of the caisson's better attitude during the fourth construction (Wang et al. 2021), data from the fourth stage of the sinking were chosen in this study, as shown in Figure 3.

The sidewall earth pressure at the depths from 33.74 m to 37.94 m is shown in Figure 4. The effect of the caisson step on the sidewall soil pressure starts to decrease with the increase in caisson depth.

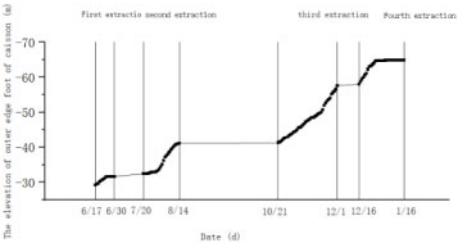

Figure 3. Elevation curve of caisson.

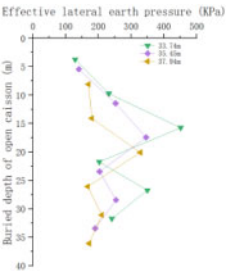

Figure 4. Curve of sidewall soil pressure with sinking depth.

4 A NEW CALCULATION MODEL OF SIDEWALL SOIL PRESSURE

On the basis of the geotechnical engineering and monitoring data of the caisson foundation of the Changtai Yangtze River Bridge, a new distribution model of sidewall soil pressure was proposed, with reference to the existing calculating model of sidewall soil pressure. Furthermore, this model considered the stress relaxation effect at the bottom of the caisson, as shown in Equations (1) and (2) and Figure 5.

$$\left.\begin{aligned} E &= \gamma h K_Z \quad h \le \tfrac{1}{2}H \\ E &= \gamma K_Z H - h \quad \tfrac{1}{2}H < h \le \tfrac{2}{3}H \\ E &= \gamma \tfrac{1}{3} H K_Z \quad \tfrac{1}{2}H < h \le H \end{aligned}\right\} \tag{1}$$

$$\gamma = \frac{\sum_{i=1}^{n} \gamma_i h_i}{\sum_{i=1}^{n} h_i} \Bigg\} \tag{2}$$

Where H is the total sinking depth, γ is the average floating weight, H_t is the depth of the footing step into the earth, and α is the discount factor of the sidewall friction above the step of the well wall, which is related to the nature of the stratum soil. Based on the measured data and compared with the calculated values of static and passive earth pressure, $K_Z$was selected as 0.5 times the

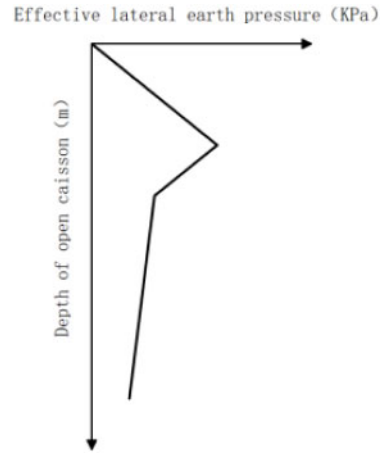

Figure 5. Sidewall soil pressure of the proposed model.

passive earth pressure. The effective earth pressure at the sidewall calculated from the above model is compared with the measured earth pressure. From Figure 6, it can be seen that the calculated and measured values of the sidewall soil pressure are well consistent.

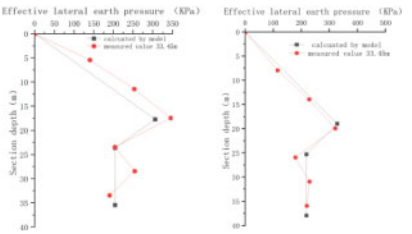

(a) Depth of 33.45 m (b) Depth of 37.94 m

Figure 6. Comparison between measured and calculated values.

5 CONCLUSIONS

1. The measured data of the sidewall soil pressure of the caisson foundation showed that the steps of the caisson foundation exhibit significant reduction effect on the sidewall soil pressure above and below the step.
2. In addition, the relaxation effect and the influence range are increased considerably as the sinking depth increases, and both the caisson step effect on soil pressure and the relaxation effect on the pressure of the ground are considered.
3. A new sidewall soil pressure calculation model was proposed in line with the existing sidewall soil pressure distribution model, which provides an important reference for the sidewall soil pressure of similar large caisson foundations.

REFERENCES

Chen, X.P, Qian, P.Y, Zhang, Z.Y. (2005) Study on penetration resistance distribution characteristic of sunk shaft foundation[J]. Chinese Journal of Geotechnical Engineering, 27(2). 148–152 (in Chinese)

Chen, X.Z, Ye, J. Geotechnical Engineering[M]. Tsinghua University publishing house Co., Ltd.
Guo, M.W, Dong X.C, Shen, K.J et al. (2021) Study on the variation of the bottom resistance during sinking stage of super large caisson foundation[J]. Chinese Journal of Rock Mechanics and Engineering, 40(1). 2977–2985 (in Chinese)
He, Q.L, Wei, R.M, Xiong, H et al. (2020) Calculation and analysis of the side friction of caisson foundation[J]. Construction Technology, 49.1715–1719 (in Chinese)
Jiang, B.L, Ma, J.L, Chu, J.L et al. (2019) On-site monitoring of lateral pressure of ultra-deep large and subaqueous open caisson during construction[J]. Rock and Soil Mechanics, 40(4). 1551–1560 (in Chinese)
Qin, S.Q, Tan, G.H, Lu, Q.F et al. (2019) Research on Design and Sinking Method of Super large Caisson Foundation[J]. Bridge Construction, 50(5).1–9 (in Chinese)
Shi, Z, Li, S.Y, Yang, S.L et al. (2019) Study on the characteristics of friction resistance and the mechanism of sudden sinking in the middle and late sinking stages of super large caisson foundation[J]. Chinese Journal of Rock Mechanics and Engineering, 38(2). 3894–3904 (in Chinese)
Wang, Z.C, Yang, Q, Chen, J.R et al. (2021) Monitoring data analysis of super large underwater steel open caisson construction[J]. Journal of China & Foreign Highway. (in Chinese)
Zhang, K, Ma, J.L, Zhou, H.X et al. (2019) Seismic response law of large span railway cable-stayed bridge under non-uniform excitation[J]. Railway Engineering, 59(6). 28–32 (in Chinese)
Zhou, H.X, Ma, J.L, Zhang, K et al. (2018) Experimental study of distribution characteristics of friction resistance on sidewall of open caisson[J]. Bridge Construction, 48(5). 27–32 (in Chinese)

Frontiers of Civil Engineering and Disaster Prevention and Control – Yang & Rahman (Eds)

Experimental research on local outburst prevention effect of coal road driving

Zhonghua Wang*
National Key Laboratory of Gas Disaster Detecting, Preventing and Emergency Controlling, Chongqing, China
China Coal Technology Engineering Group Chongqing Research Institute, Chongqing, China

ABSTRACT: In order to study the local outburst prevention effect of coal roadway driving, the cuttings index method is used to predict the outburst risk of coal roadway driving and the effect is tested in the process of coal roadway driving. At the same time, the gas concentration after the blasting of coal roadway excavation is analyzed statistically, which verifies the accuracy of outburst prediction and effect inspection of coal roadway excavation so as to ensure the safe excavation of coal lanes.

1 INTRODUCTION

Shangzhuang Minefield is a part of the Wusheli mining area in Fengcheng Hexi Coalfield, located in Fengcheng City in the middle and lower reaches of the Ganjiang River. The mine is about 5.1 km long, about 2.65 km wide, and has an area of about 13.288 km^2. The approved production capacity in 2005 was 350 kt/a, and the annual output has stabilized at 350,000 to 400,000 tons in recent years. The main geological factors affecting the zoning of Shangzhuang Coal Mine gas are: coal seam burial depth, coal seam thickness, coal seam gas storage conditions, regional geological structure, etc. The gas pressure test results are shown in Table 1. This paper aims to test the local sensitivity index of coal roadway precisely, which is of great importance to the safe excavation of coal roadway.

Table 1. Measurement result of gas pressure.

Measurement location	See coal elevation (m) Gas pressure (MPa)	See coal elevation (m) Gas pressure (MPa)
710 Floor Roadway	−622.5	6.0
505 Floor Roadway	−783	2.0

2 OUTBURST PREDICTION METHOD OF COAL ROAD EXCAVATION

2.1 *Prediction of outburst hazard in coal road excavation*

After the outburst prevention measures are implemented on the coal roadway driving face, the drill cuttings index method is used to predict the outburst risk of the coal roadway driving face. At least

*Corresponding Author: boaidajia2007@126.com

 DOI 10.1201/9781003308577-7

three boreholes with a diameter of 42 mm and a hole depth of 8–10 m should be constructed on the coal seam face toward the front coal body (Chen et al. 2019; Li et al. 2020). Determine the drill cuttings' gas desorption index and the amount of drill cuttings. Drill holes should be arranged in soft layers as much as possible. One hole is located in the middle of the tunnel section and parallel to the direction of excavation. The final hole points of other drill holes should be located 4 m outside the contour line on both sides of the tunnel section. The total amount of cuttings S of the 1 m section is measured every 1 m of the borehole, and the value of the gas desorption index of drill cuttings K1 is measured at least once every 2 m of the drilling. When the drilling cuttings index method is used to predict the outburst hazard of a coal tunnel driving face, the outburst hazard critical value of each index is shown in Table 2.

Table 2. Critical value of drilling cuttings index method to predict the outburst risk of coal roadways.

Drill cuttings gas desorption index K1 ($mL/g{\cdot}min^{1/2}$)	Drilling cuttings S (kg/m)
Dry coal sample < 0.5 Wet coal sample < 0.4	<6 (Aperture Φ42 mm)

2.2 *Outburst prevention effect test of coal tunnel driving*

In the event that the working face is predicted to be one free of outburst hazards, the driving drill cutting index method is used to test the effectiveness of coal tunnel driving measures.

2.2.1 *Indicators and critical values*

Normal coal seam critical index K1 value is 0.5 $mL/g{\cdot}min^{1/2}$, Smax value is 6 kg/m; fault structure zone (20 m before and after the structure), coal seam thickness change zone, stress concentration zone K1 critical value is 0.4 $mL/g{\cdot}min^{1/2}$, Smax value is 6 kg/m.

2.2.2 *Inspection steps*

(1) After the discharge drilling is completed, the effect inspection will be carried out. Three effect inspection holes are constructed in the middle of the measure holes. The hole depth is 10 m, the diameter is 42 mm, and the control area is 4 m outside the contour line of the roadway, which is arranged in a fan shape (Mao et al. 2019; Li. & Jiang 2019).
(2) When $K1 < 0.5$ $mL/g{\cdot}min^{1/2}$ and $S < 6$ kg/m, the prevention and control measures are considered effective. According to the design of intensive drilling, ensure an advance distance of 5 m in front of the roadway (calculated by projection), and the allowable footage is 4.5 m.
(3) In the 20 m before and after the fault structure zone and the geological structure change zone, when $K1 = 0.4$ $mL/g{\cdot}min^{1/2}$ and $S = 6$ kg/m, only a small loop footage can be allowed, i.e., a maximum of 1.5 m per sub-shift. The leading distance must be kept at 7 m.
(4) If $K1 = 0.5$ $mL/g{\cdot}min^{1/2}$ or $S = 6$ kg/m, the inspector must drill a number of counter holes beside the inspection hole of the supercritical index according to the inspection drilling situation, and then an effect inspection is carried out between the supplementary drilling measures. If the effectiveness inspection holes meet the requirements of the hole layout and the three sets of effectiveness inspection indicators are not supercritical, the prevention and control measures are considered effective; otherwise, the regional outburst prevention measures must be taken again (Wang et al. 2017).
(5) When the inspection result measures are effective, if the projected length of the inspection hole and the anti-outburst drill hole in the direction of roadway driving (referred to as the projected hole depth) is equal, the conditions that allow sufficient anti-outburst measures to advance and take safety protection measures during down digging At the same time, when the depth of the projection hole of the inspection hole is less than the hole of the anti-outburst measure, it shall

be implemented after taking safety protection measures under the condition that the required advance distance of the anti-outbreak measure is reserved and at the same time there is at least 2m of the inspection hole projection hole depth.

3 OUTBURST PREVENTION EFFECT TEST OF COAL TUNNEL DRIVING

3.1 *Analysis of coal tunnel driving index*

The outburst hazard prediction in Shangzhuang Coal Mine's coal roadway was tested during the tunneling process. The inspection results of K1 and S indicators are shown in Table 3, and the indicator change curve is shown in Figure 1.

Table 3. K1 and S statistics of coal roadway driving efficiency inspection index.

Total footage (m)	Drilling diameter (mm) Size	Drill cuttings desorption index K1 (mL/g·min$^{1/2}$)		Cuttings S (kg/m)	
		Excess (number)	Size	Excess (number)	
176	75	0.08–0.43	0	2–4.7	0

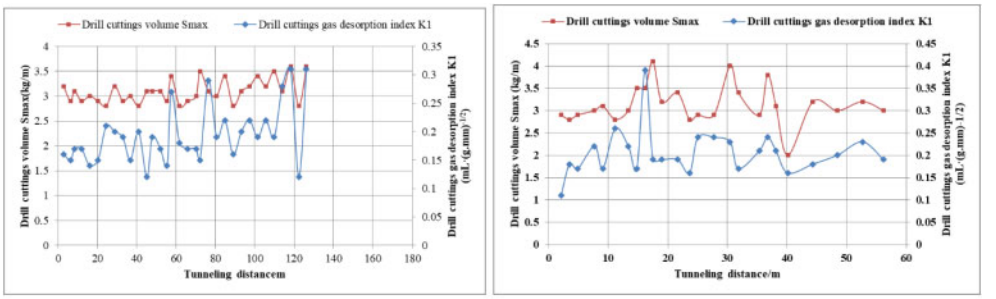

(a) 710 coal road (b) 505 coal road

Figure 1. K1 and S prediction indexes of coal road excavation.

It can be seen from Figure 1 that after the coal roadway adopts the regional measures of floor pressure relief rock roadway combined with cross-layer borehole pre-drainage coal roadway strip gas, the K1 and S prediction indexes are both small, and the drilling cuttings gas desorption index K1 value is 0.08–0.43 mL/g·min$^{1/2}$, which is less than the critical value 0.5 mL/g·min$^{1/2}$, and the drill cuttings S value is 2–4.7 kg/m, which is less than the critical value of 6 kg/m, realizing safe excavation of coal roads.

3.2 *Analysis of gas concentration after blasting in Coal roadway driving*

In order to ensure the safety of coal tunnel excavation, in the process of coal tunnel excavation, the gas concentration of Shangzhuang Coal Mine's test roadway after blasting was carried out to verify the accuracy of the coal tunnel effect. The gas concentration change curve is shown in Figure 2.

It can be seen from Figure 2 that the gas concentration in the coal roadway is between 0.12% and 0.73% after the blasting. No gas has appeared since the coal roadway adopted the regional measures of floor pressure relief rock roadway combined with through-bed drilling and pre-draining coal road strip gas. Over-limit phenomenon. The coal tunnel demonstrates a safe excavation method in order to verify the danger of the coal tunnel excavation effect test.

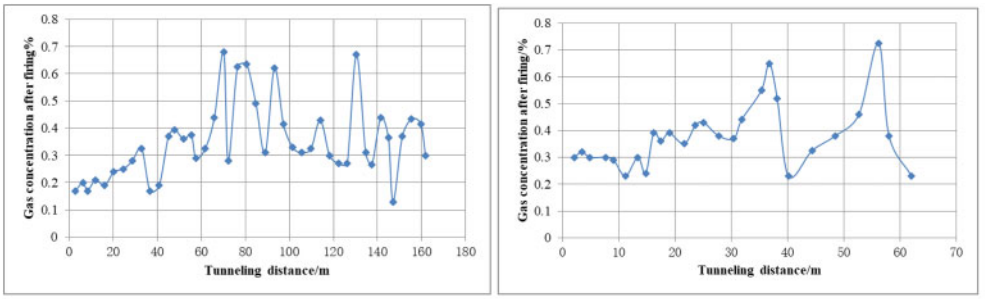

(a) 710 coal road (b) 505 coal road

Figure 2. Concentration change curve after blasting in coal roadway excavation.

4 CONCLUSION

Following the adoption of the regional measures of pressure relief rock roadway and drilling through the layer to pre-drain the coal roadway strip gas, both the K1 and S prediction indices are small, and both are less than the critical value of outburst risk from coal roadway excavation.

The gas concentration in the coal roadway was between 0.12% and 0.73% after the blasting, and there was no gas over-limit phenomenon, which verified the danger of the coal roadway driving effect test and the coal roadway realized safe driving.

ACKNOWLEDGMENTS

This work was financially supported by the Tiandi Technology Co., Ltd. Special Project of Science and Technology Innovation and Entrepreneurship Fund (Grant No. 2021-2-TD-ZD008), and Chongqing Natural Science Foundation General Project (Grant No. cstc2021jcyj-msxmX1149).

REFERENCES

Chen X.X., Zhang P.G., Hou F.J. (2019) Chen Guangjian. Determination of sensitive index and critical value for coal seam outburst prediction in a mine of Xin'an Coal Field[J]. Journal of North China Institute of Science and Technology, 16(06): 1–6.

Li Y., Zhang Y., Qin Z. (2020) Research on determination of sensitive indexes for coal and gas outburst prediction in Hexi coal mine[J]. Energy Technology and Management, 45(04): 143–145.

Li Y.H., Z.K., Jiang H. (2019) Experimental research on sensitive indicators of local outburst prediction in coal mines[J]. Energy and Environmental Protection, 41(09): 1–4+9.

Mao J.N., Wang S.L., Jiang Q.F. Chen Chunyuan. (2019) Determination of the critical value of outburst prediction sensitivity index for coal roadway driving face[J]. China Mining Industry, 28(S1): 150–153.

Wang J.S., Zhang Y.M., Fan H.M. (2017) Determination of sensitive indexes and critical values of driving faces[J]. China Coal, 43(07): 131–133.

Frontiers of Civil Engineering and Disaster Prevention and Control – Yang & Rahman (Eds)

Research on design and experimental application of flexible pavement base

Jianping Su*
China Urban and Rural Holding Group Co., Ltd., Beijing, China

ABSTRACT: In recent years, with the increase in traffic volume and heavy vehicles, asphalt pavement has prematurely shown problems such as fatigue cracking and insufficient rutting resistance. The commonly used mixture structure of asphalt pavement cannot adapt to the growing volume of traffic and heavy traffic situations. It has become an urgent and important task to study new pavement structures. This paper presents the design and experimental performance evaluation of flexible base pavements, analyses of the relevant performance indicators of different flexible pavement structures, as well as construction suggestions that could be applied to practical applications. The research result shows that the engineering effect is good.

1 INTRODUCTION

In recent years, with the increase of traffic volume, heavy vehicles and the influence of traffic channelization, asphalt pavement has shown shortcomings such as premature fatigue cracking and insufficient anti-rutting ability, which reduce the performance of the pavement, shorten the service life of the pavement, and greatly increase the cost of reconstruction and maintenance. The commonly used mixture structure of asphalt pavement cannot adapt to the growing volume of traffic and heavy traffic situations. It has become an urgent and important task to study new pavement structures (Hardy & Cebon 1994; Liu 2002; Zaghloul & White 1993). Meanwhile, it is of great practical significance to adopt a flexible base structure to improve the high and low-temperature performance of asphalt pavement and intensify the water loss and fatigue resistance of the asphalt mixture. In this paper, the design and experimental application of the flexible pavement base of the Qingdao-Yinchuan Expressway from Jilujie to Shijiazhuang are studied and analyzed. Additionally, the paving of the road has been tested on the flexible base of the road section, and the engineering application has demonstrated a good effect.

2 PROJECT OVERVIEW

The Qingdao-Yinchuan Highway from Jilujie to Shijiazhuang is an organizational part of the "five north-to-south longitudinal superhighways and seven east-to-west transverse superhighways" national highway trunk lines planned by the Ministry of Communications. According to the current traffic volume forecast results and considering the status and role of the project in the road network, it is planned to adopt the standard construction of expressways. The driving speed is calculated at 120 km/h, and the design load of the bridge and culvert adopts the automobile-super-20 level and the hanging-120. The roadbed is 28 meters wide, with four lanes in both directions, which are fully enclosed and fully interchangeable. The total length of the expressway from Jilujie to the Shijiazhuang section of the Qingdao-Yinchuan Highway is 183.551 kilometers, and the total length of the research section is 18.79 kilometers.

*Corresponding Author: sujianping0104@163.com

 DOI 10.1201/9781003308577-8

3 RESEARCH ON FLEXIBLE BASE DESIGN

The design idea of the flexible base comes from the American practice of using asphalt stabilized gravel or graded gravel as the base on the semi-rigid base and then laying the asphalt concrete surface. Generally, in the pavement structure, the upper layer of the pavement is defined as the functional layer, and the middle and lower layers, as well as the base layer, are defined as the load-bearing layers of the structure. Moreover, flexible base pavement usually has two typical structures. One is a full-thickness flexible pavement, that is, the upper, lower base, and surface layers are asphalt mixture, and the total thickness of the asphalt layer is thick, which is also called a permanent pavement structure, and the other type is a hybrid flexible pavement, which has two types. One is to pave the flexible transition base on the semi-rigid base, and the other is to take the graded gravel as the lower base, and then to pave the asphalt surface, which is also known as the inverted structure or sandwich structure (Lv 2006).

Combined with the traffic characteristics, regional characteristics, and research needs of the project, coarse-grained asphalt macadam is used as the base material in this experiment, and full-thickness and hybrid structures are adopted in the structural form. The length of a hybrid pavement structure is 8.96 km (half), and the length of a full-thickness pavement structure is 5.769 km (half). The specific structural design is shown in Table 1.

Table 1. Structure design of flexible base pavement.

Structure type	Hybrid structure	Full-thickness structure
Stationary paragraph	K129+320-K138+280 left	K119+490-K125+259 right
Upper layer	4 cm fine-grained asphalt concrete SAC-13 SBR modified emulsified asphalt sticky layer	4 cm fine-grained asphalt concrete SAC-13 SBR modified emulsified asphalt sticky layer
Middle layer	6 cm medium grain asphalt concrete AC-20 SBR modified emulsified asphalt sticky layer	6 cm medium grain asphalt concrete AC-20 SBR modified emulsified asphalt sticky layer
Lower layer	6 cm coarse-grained asphalt concrete AC-25	6 cm coarse-grained asphalt concrete AC-25
Up-sealing layer	Thermal spray modified asphalt plus crushed stone seal	SBR modified emulsified asphalt sticky layer
Upper level	12 cm coarse-grained asphalt stabilized crushed stone LSM-30 SBR modified emulsified asphalt sticky layer transparent layer	16 cm coarse-grained asphalt stabilized crushed stone BL1-30 SBR modified emulsified asphalt sticky layer 17 cm coarse-grained asphalt stabilized crushed stone BL1-30
Lower level	18 cm cement stabilized and crushed stone	5-6 mm emulsified asphalt slurry seal
Sub-base	18 cm cement lime stabilized soil	15 cm lime-fly ash stabilized aggregate treatment soil foundation 18 cm cement lime soil treatment soil foundation